Топологические изоляторы и смежные вопросы

Школа ИТЭФ - 2011

М.В.Фейгельман

ИТФ им. Л.Д.Ландау

План лекций

Лекция 1 - Введение

- Что такое топологические изоляторы
- Известные экспериментальные объекты
- Эксперименты (ARPES, STM, электр.транспорт)

Лекция 2 - Кое-что о теории

- Топологические свойства зонных диэлектриков
- Общая классификация топологических фаз
- Связь с проблемами спиновой жидкости и p_x+ip_y сверхпроводящего состояния
- Майорановские фермионы: как напасть на их след

Что такое топологич. изолятор - 1

- Простейший пример: зонный диэлектрик (3-мерный или 2-мерный), образующий поверхностные проводящие состояния
- Обобщение: любая система со щелью в спектре в объёме, но безщелевыми состояниями на поверхности (например, сверхтекучий ^{3}He-B)

Предистория:

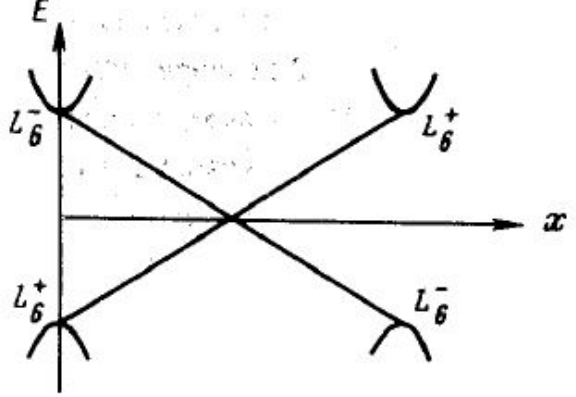

Рис. 1. Инверсия зон $L_6^{\pm}$ в $Pb_{1-x}Sn_xTe(Se)$

Письма в ЖЭТФ, том 42, вып. 4, стр. 145 – 148 *25 августа 1985 г.*

БЕЗМАССОВЫЕ ДВУМЕРНЫЕ ЭЛЕКТРОНЫ В ИНВЕРСНОМ КОНТАКТЕ

Б.А.Волков, О.А.Панкратов

Предложен новый тип полупроводниковых структур на основе контакта двух материалов с взаимно инвертированными зонами. Качественной особенностью такого контакта является наличие в нем независящих от вида переходной области электронных состояний с линейным двумерным спектром. Определены свойства инверсного контакта во внешнем магнитном поле.

В двухзонном приближении энергетический спектр такого контакта описывается уравнением Дирака с зависящей от координаты z шириной запрещенной зоны:

$$\begin{pmatrix} -\epsilon & i\epsilon_g/2 + \vec{\sigma}\mathbf{p} \\ -i\epsilon_g/2 + \vec{\sigma}\mathbf{p} & -\epsilon \end{pmatrix} \begin{pmatrix} \chi_- \\ \chi_+ \end{pmatrix} = 0, \qquad (1)$$

где $\vec{\sigma}$ – матрицы Паули, $\mathbf{p} = -i\hbar(v_\perp \nabla_x, v_\perp \nabla_y, v_\parallel \nabla_z)$, ось z направлена по тригональной оси кристалла, $\chi_\pm$ – двухкомпонентные спиноры. Если по разные стороны контакта знаки ϵ_g различны ($\epsilon_g(-\infty) < 0, \epsilon_g(+\infty) > 0$), то независимо от конкретного вида функции $\epsilon_g(z)$ всегда существуют два локализованных у контакта решения уравнения (1):

$$\Psi_\pm = A \begin{pmatrix} \pm \exp(-i\theta/2) \\ 0 \\ 0 \\ \exp(i\theta/2) \end{pmatrix} \exp\left\{ -\frac{1}{2\hbar v_\parallel} \int_0^z \epsilon_g(z)dz + i\mathbf{k}_\perp \mathbf{r} \right\}, \qquad (2)$$

где $\mathbf{k}_\perp = (k_x, k_y, 0)$, $\exp(i\theta) = (k_x + ik_y)/k_\perp$. Подстановкой (2) в (1) можно убедиться, что в плоскости (x, y) функции $\Psi_\pm$ удовлетворяют уравнению Дирака с нулевой массой, унитарно эквивалентному уравнению Вейля. Соответствующий невырожденный безмассовый спектр

$$\epsilon_0^\pm(\mathbf{k}_\perp) = \pm \hbar v_\perp k_\perp \qquad (3)$$

Гамильтониан поверхностных электронных состояний

- $H = v_0(-i\underline{\partial} - e\underline{A})\underline{\sigma} + g_{eff}\underline{\sigma B}$

двумерный градиент вдоль поверхности

зеемановский член

Щель в спектре пропорциональна $g_{eff}B_z$

Сравним с графеном:

- один «дираковский» фермион вместо 4-х в графене (там 2 долины и 2 проекции спина) Не работает теорема удвоения !
- Псевдоспин из ур-ния Дирака – это «почти» реальный спин электрона (в графене – это индекс подрешеток, не связанный со спином)
- Поэтому магнитное поле $\perp$ поверхности открывает щель в спектре

Quantum Spin Hall Insulator State in HgTe Quantum Wells

Markus König,[1] Steffen Wiedmann,[1] Christoph Brüne,[1] Andreas Roth,[1] Hartmut Buhmann,[1] Laurens W. Molenkamp,[1*] Xiao-Liang Qi,[2] Shou-Cheng Zhang[2]

Новая история: *Science* **318** 766 (2007)

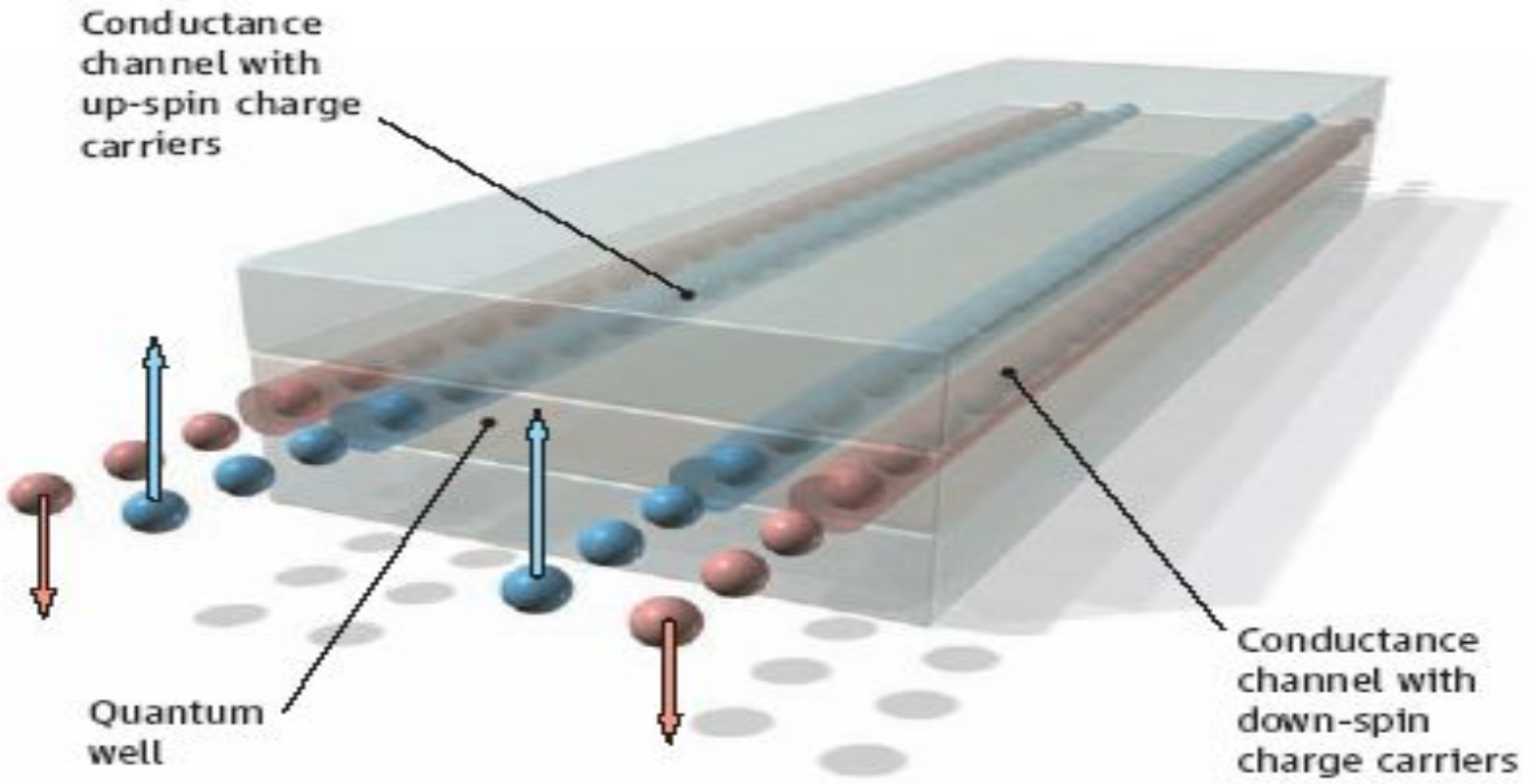

Schematic of the spin-polarized edge channels in a quantum spin Hall insulator.

$$H_{\text{eff}}(k_x,k_y) = \begin{pmatrix} H(k) & 0 \\ 0 & H^*(-k) \end{pmatrix},$$

$$H = \varepsilon(k) + d_i(k)\sigma_i$$

$$d_1 + id_2 = A(k_x + ik_y) \equiv Ak_+$$

$$d_3 = M - B(k_x^2 + k_y^2),$$

$$\varepsilon_k = C - D(k_x^2 + k_y^2).$$

M < 0 leads to surface anomaly

Recent theory predicted that the quantum spin Hall effect, a fundamentally new quantum state of matter that exists at zero external magnetic field, may be realized in HgTe/(Hg,Cd)Te quantum wells. We fabricated such sample structures with low density and high mobility in which we could tune, through an external gate voltage, the carrier conduction from n-type to p-type, passing through an insulating regime. For thin quantum wells with well width $d < 6.3$ nanometers, the insulating regime showed the conventional behavior of vanishingly small conductance at low temperature. However, for thicker quantum wells ($d > 6.3$ nanometers), the nominally insulating regime showed a plateau of residual conductance close to $2e^2/h$, where e is the electron charge and h is Planck's constant. The residual conductance was independent of the sample width, indicating that it is caused by edge states. Furthermore, the residual conductance was destroyed by a small external magnetic field. The quantum phase transition at the critical thickness, $d = 6.3$ nanometers, was also independently determined from the magnetic field–induced insulator-to-metal transition. These observations provide experimental evidence of the quantum spin Hall effect.

Краевые состояния не имеют рассеяния назад

No back-scattering !

- Спин однозначно связан с импульсом:

|1>

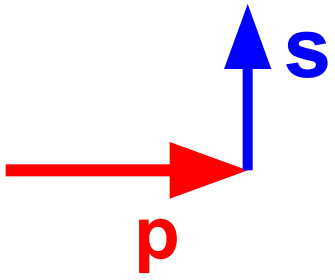

|2>

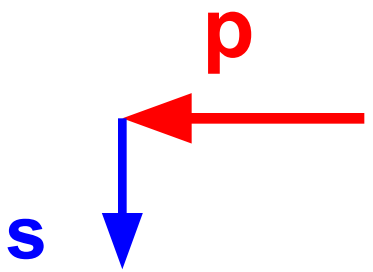

<1|2> = 0 *если нет явно спин-зависящего взаимодействия*

Что такое топологич. изолятор - 2

Электродинамика с Θ-членом:

$$\Delta L_{axion} = \theta(e^2/2\pi hc)\mathbf{B}\cdot\mathbf{E}$$

Θ = π (2n+1) для сохранения T-инвариантности

$$S_{3D} = \frac{2n+1}{8\pi}\int d^3x dt \epsilon^{\mu\nu\sigma\tau}\partial_\mu A_\nu \partial_\sigma A_\tau .$$

$\exp(iS_{3D}) = (-1)^n$

для интеграла по замкнутому пространству

(изложение по материалу M. Franz, Physics **1**, 36 (2008)

Что будет при $\Theta \neq$ CONST ?

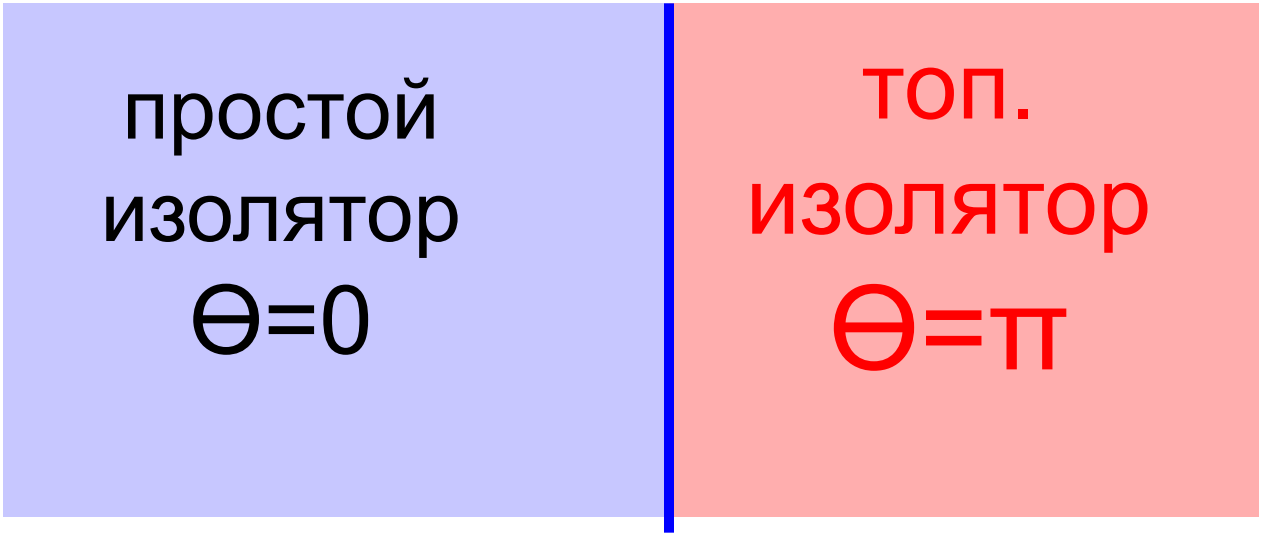

$$\nabla \cdot \mathbf{E} = \rho - (e^2/2\pi\hbar c)\nabla\theta \cdot \mathbf{B}$$

$$\nabla \times \mathbf{B} = \partial_t \mathbf{E} + \mathbf{j} + (e^2/2\pi hc)(\nabla\theta \times \mathbf{E} + \partial_t\theta \mathbf{B})$$

Аномальные члены сидят на границе

Т-инвариантность там нарушена

Магнито-электрический эффект

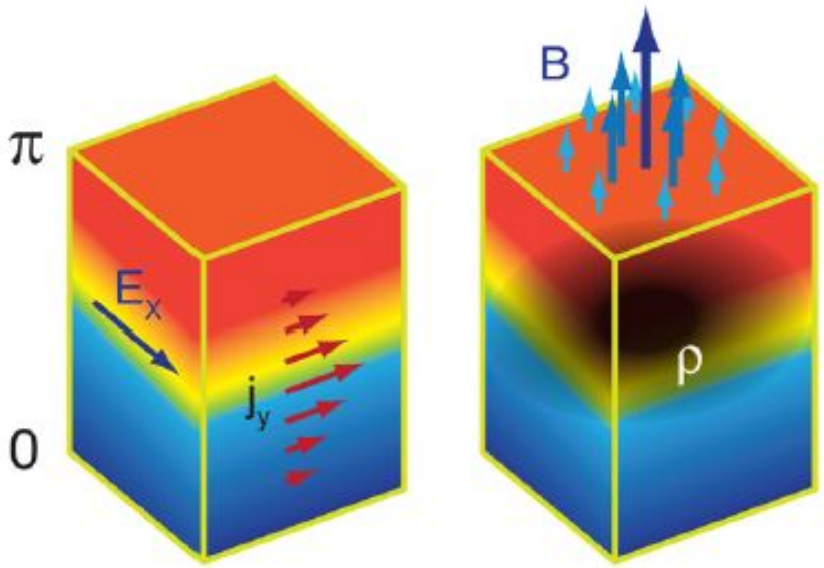

A magnetic field applied perpendicular to the same interface introduces $(n + 1/2)$ electrons for each flux quantum of applied field. The shaded region corresponds to the charge density, ρ, of the electrons, which mainly concentrates around the boundary between the two insulators and is largest where the magnetic field is strongest. (Illustration: Alan Stonebraker/`stonebrakerdesignworks.com`)

(Left) A quantum Hall effect occurs without strong magnetic field when an electric field applied in the plane of the interface between a topological (red region) and an ordinary (blue region) insulator (or vacuum) induces a precisely quantized current perpendicular to the field. (Right)

$$\sigma_{\mathrm{H}} = (e^2/h)(n + 1/2)$$

Кроме того,
эффект Керра –
вращение плоскости
поляризации
отраженного света

"Dynamical Axion Field in Topological Magnetic Insulators"

R. LiR. Li, J. WangR. Li, J. Wang, X. QiR. Li, J. Wang, X. Qi, S.-C. Zhang

- Axions are very light, very weakly interacting particles postulated more than 30 years ago in the context of the Standard Model of particle physics. Their existence could explain the missing dark matter of the universe. However, despite intensive searches, they have yet to be detected. In this work, we show that magnetic fluctuations of topological insulators couple to the electromagnetic fields exactly like the axions, and propose several experiments to detect this dynamical axion field. In particular, we show that the axion coupling enables a nonlinear modulation of the electromagnetic field, leading to attenuated total reflection. We propose a novel optical modulators device based on this principle.

Arxiv: **0908.1537**

Объекты, известные как Топологические Изоляторы или Топ. Сверхпроводники

- 2D: HgTe (квантовые ямы с 2D электронами)
- 3D: $Bi_{1-x}Sb_x$ Bi_2Se_3 Bi_2Te_3 $Tl\,Bi\,Se_2$
- ^{3}He-B Н.Копнин et al J.LowTemp.Phys. 85, 267 (1991)

  Г.Воловик Письма ЖЭТФ 90, 440 (2009).

  Topological superfluid ^{3}He-B: fermion zero modes on interfaces and in the vortex core M.A. Silaevin the vortex core M.A. Silaev, G.E. Volovik arXiv:1005.4672

Эксперименты ARPES

nature Vol 452|24 April 2008|doi:10.1038/nature06843

LETTERS

A topological Dirac insulator in a quantum spin Hall phase

D. Hsieh[1], D. Qian[1], L. Wray[1], Y. Xia[1], Y. S. Hor[2], R. J. Cava[2] & M. Z. Hasan[1,3]

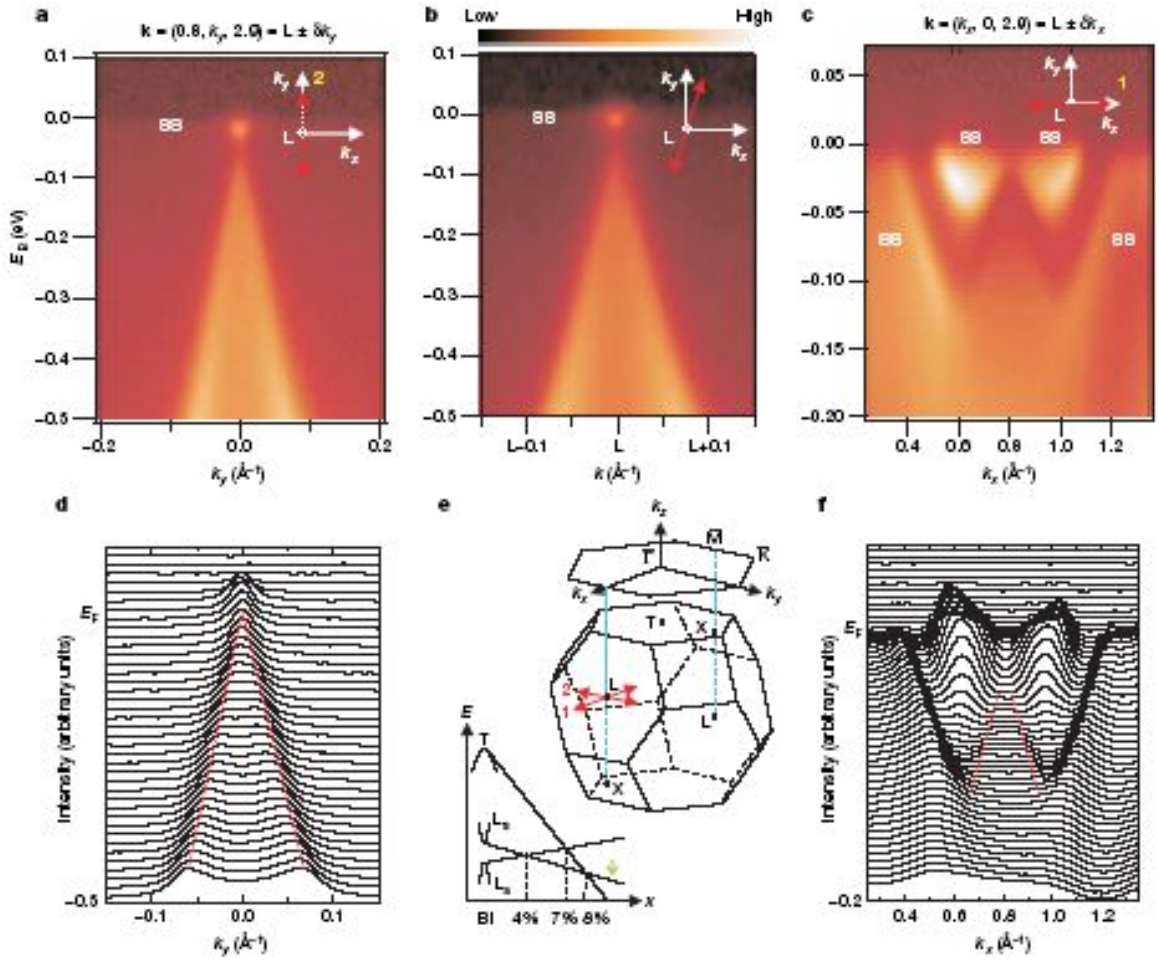

Figure 1 | Dirac-like dispersion near the L-point in the bulk Brillouin zone. Selected ARPES intensity maps of $Bi_{0.9}Sb_{0.1}$ are shown along three **k**-space cuts through the L-point of the bulk 3D Brillouin zone. The presented data are taken in the third Brillouin zone with $L_z = 2.9\,\text{Å}^{-1}$ with a photon energy of 29 eV. The cuts are along the k_y-direction (**a**); a direction rotated by approximately 10° from the k_y-direction (**b**); and the k_x-direction (**c**). Here, δ symbolizes a change along a particular **k**-direction. Each cut shows a Λ-shaped bulk band whose tip lies below the Fermi level, signalling a bulk gap. The surface states are denoted SS and are all identified in Fig. 2 (for further identification via theoretical calculations, see Supplementary Information). **d**, Momentum distribution curves corresponding to the intensity map in **a**. **f**, A log-scale plot of the momentum distribution curves corresponding to the intensity map in **c**. The red lines are guides to the eye for the bulk features in the momentum distribution curves. **e**, Schematic of the bulk 3D Brillouin zone of $Bi_{1-x}Sb_x$ and the 2D Brillouin zone of the projected (111) surface. The high-symmetry points $\bar{\Gamma}$, $\bar{M}$ and $\bar{K}$ of the surface Brillouin zone are labelled. The schematic evolution of bulk band energies as a function of x is shown. The L-band inversion transition occurs at $x \approx 0.04$, where a 3D gapless Dirac point is realized, and the composition we study here (for which $x = 0.1$) is indicated by the green arrow. A more detailed phase diagram based on our experiments is shown in Fig. 3c.

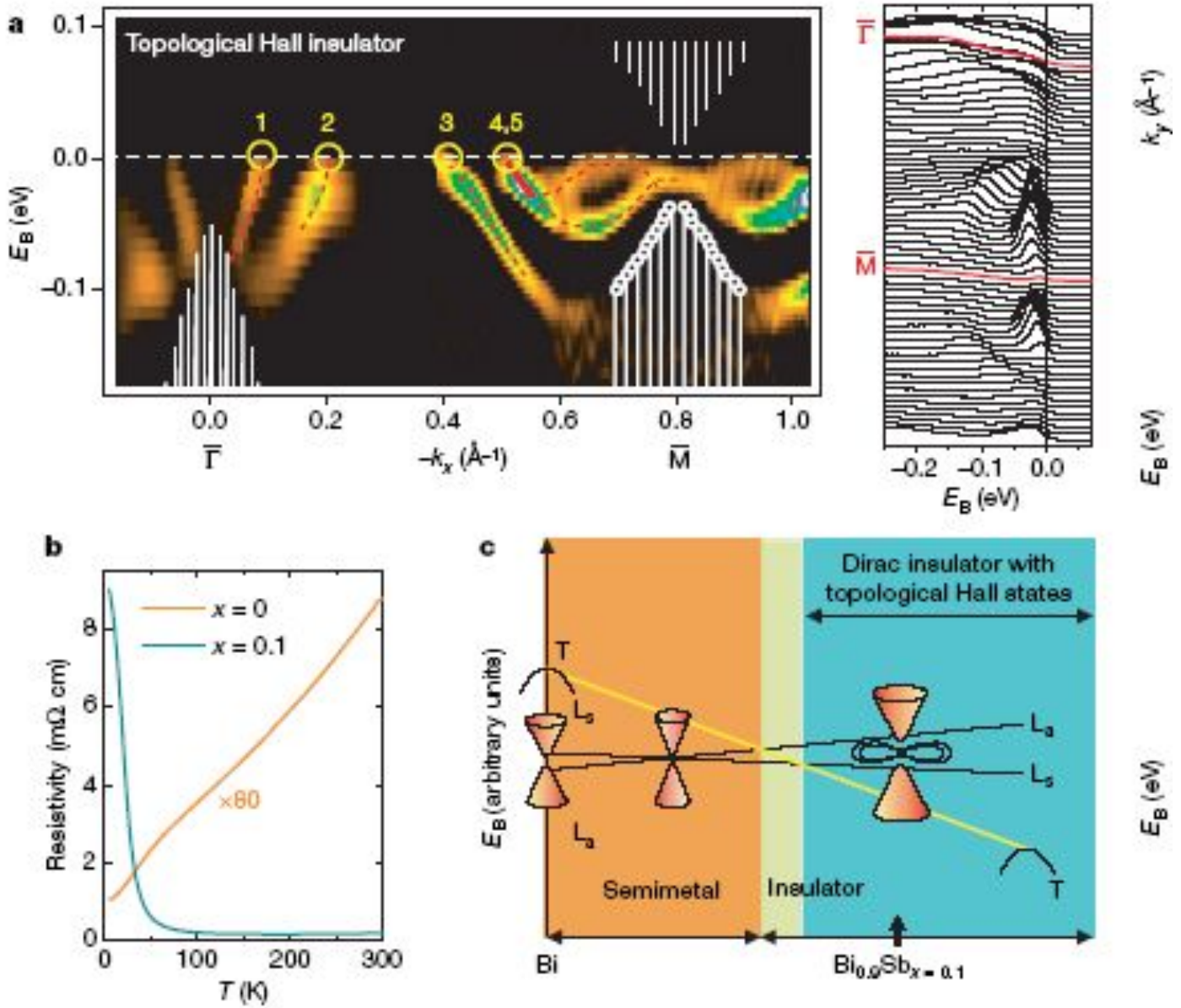
a
Topological Hall insulator
1
2
3
4,5
0.1
0.0
−0.1
E_B (eV)
0.0
0.2
0.4
0.6
0.8
1.0
$\bar{\Gamma}$
$-k_x$ (Å^{-1})
$\bar{M}$
$\bar{\Gamma}$
$\bar{M}$
−0.2
−0.1
0.0
E_B (eV)
k_y (Å^{-1})
E_B (eV)
b
$x = 0$
$x = 0.1$
×80
Resistivity (mΩ cm)
0
2
4
6
8
0
100
200
300
T (K)
c
Dirac insulator with
topological Hall states
T
L_a
L_a
L_a
T
E_B (arbitrary units)
Semimetal
Insulator
Bi
$Bi_{0.9}Sb_{x=0.1}$
E_B (eV)

0
8
1
2
2
0
7
8

Electrons on the surface of Bi_2Se_3 form a topologically-ordered two dimensional gas with a non-trivial Berry's phase

Y. Xia,[1] L. Wray,[1] D. Qian,[1] D. Hsieh,[1] A. Pal,[1] H. Lin,[2] A. Bansil,[2] D. Grauer,[3] Y. S. Hor,[3] R. J. Cava,[3] and M. Z. Hasan[1,4]

[1] *Joseph Henry Laboratories of Physics, Department of Physics, Princeton University, Princeton, NJ 08544, USA*

[2] *Department of Physics, Northeastern University, Boston, MA*

[3] *Department of Chemistry, Princeton University, Princeton, NJ 08544, USA*

[4] *Princeton Center for Complex Materials, Princeton University, Princeton, NJ 08544, USA**

recalculation

Band structure calculation

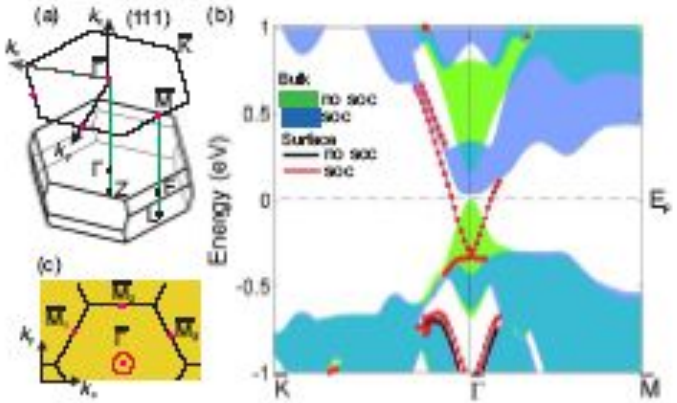

FIG. 1: Spin-orbit interaction induced surface Fermi surface: (a) A schematic of the bulk 3D BZ of Bi_2Se_3 and the 2D BZ of the projected (111) surface. (b) LDA band-structure of the 2D surface states along the $\bar{K} - \bar{\Gamma} - \bar{M}$ k-space cut. Bulk band projections are represented by the shaded areas. The band-structure results with spin-orbit coupling (SOC) is presented in blue and that without SOC is in green. No pure surface band is observed within the insulating gap without SOC (black lines). One pure gapless surface band crossing E_F is observed when SOC is included (red lines). (c) The corresponding surface FS is a single ring centered at $\bar{\Gamma}$. The band responsible for this ring is singly degenerate. The time-reversal-invariant momenta (TRIM) on the (111) surface BZ : the $\bar{\Gamma}$ and the three $\bar{M}$ points are marked by red dots.

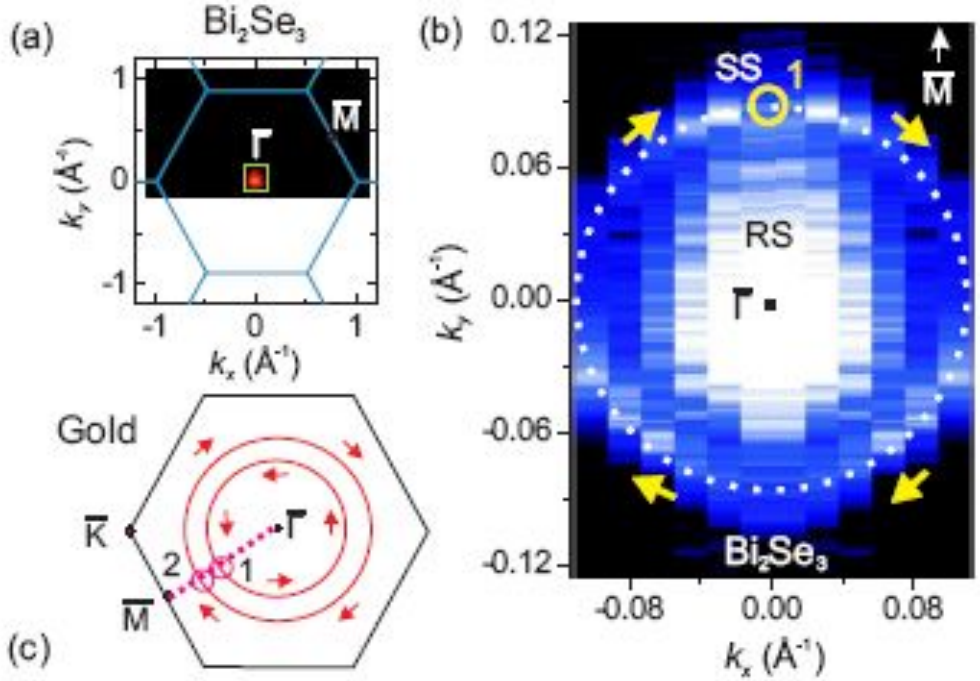

FIG. 4: The surface Fermi surface : (a) the surface FS is a small pocket around Γ. (b) High momentum resolution data around $\bar{\Gamma}$ show a single ring formed by the pure surface state band. In the middle of the ring is a filled-in disk-shaped spectral intensity reflecting resonant states (see text). The pure surface Fermi surface of BiSe is different from that of spin-orbit pair Fermi surface observed on metallic gold Au(111). (c) The Au(111) surface FS, which has two rings (each non-degenerate) surrounding the $\bar{\Gamma}$ TRIM. An electron circling the gold FS can only carry a Berry's phase of 0, characteristic of a trivial topological metal, Z_2 ==+1. The single surface Fermi surface observed in Bi_2Se_3 reflects its non-trivial topological character Z_2 =-1.

- **Large Gap Topological Insulator Bi2Te3 with a Single Dirac Cone on the Surface**

Y. L. ChenY. L. Chen, J. G. AnalytisY. L. Chen, J. G. Analytis, J. H. ChuY. L. Chen, J. G. Analytis, J. H. Chu, Z. K. LiuY. L. Chen, J. G. Analytis, J. H. Chu, Z. K. Liu, S. K. MoY. L. Chen, J. G. Analytis, J. H. Chu, Z. K. Liu, S. K. Mo, X. L. QiY. L. Chen, J. G. Analytis, J. H. Chu, Z. K. Liu, S. K. Mo, X. L. Qi, H. J. ZhangY. L. Chen, J. G. Analytis, J. H. Chu, Z. K. Liu, S. K. Mo, X. L. Qi, H. J. Zhang, D. H. LuY. L. Chen, J. G. Analytis, J. H. Chu, Z. K. Liu, S. K. Mo, X. L. Qi, H. J. Zhang, D. H. Lu, X. DaiY. L. Chen, J. G. Analytis, J. H. Chu, Z. K. Liu, S. K. Mo, X. L. Qi, H. J. Zhang, D. H. Lu, X. Dai, Z. FangY. L. Chen, J. G. Analytis, J.

[1] *Stanford Institute for Materials and Energy Sciences, SLAC National Accelerator Laboratory, 2575 Sand Hill Road, Menlo Park, California 94025*
[2] *Geballe Laboratory for Advanced Materials, Departments of Physics and Applied Physics, Stanford University, Stanford, California 94305*
[3] *Advanced Light Source, Lawrence Berkeley National Laboratory Berkeley California, 94720, USA*
[4] *Beijing National Laboratory for Condensed Matter Physics, and Institute of Physics, Chinese Academy of Sciences, Beijing 100190, China*

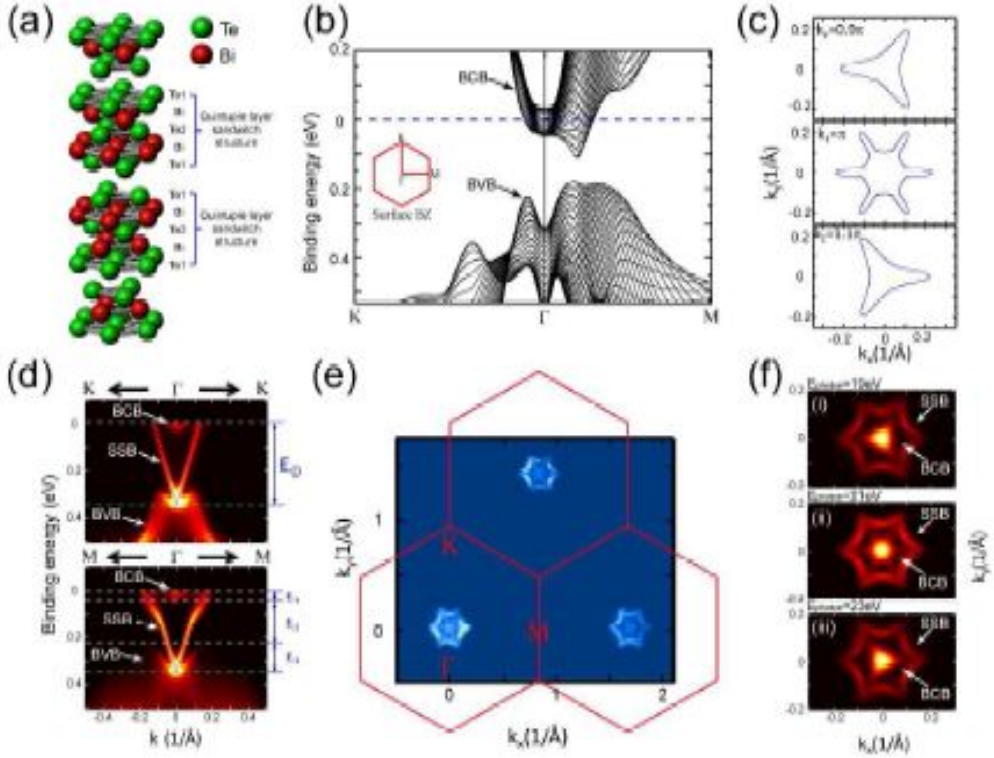

face BZ. (d) ARPES measurements of band dispersions along $K-\Gamma-K$(top) and $M-\Gamma-M$ (bottom) directions. The broad bulk band (BCB and BVB) dispersions are similar to those in panel (b), while the sharp V-shape dispersion is from the surface state band (SSB). Energy scales of the band structure are labeled as: E_0: Binding energy of Dirac point (0.34eV), E_1: BCB bottom binding energy(0.045eV), E_2:bulk energy gap(0.165eV) and E_3: energy separation between BVB top and Dirac point (0.13eV). (e) Measured wide range FS map covering three BZs shows that the FSs only exist around Γ point, where the red hexagons represent the surface BZ. The uneven intensity of the FSs at different BZs results from the matrix element effect. (f) Photon energy dependent FS maps. The shape of the inner FS changes dramatically with photon energies, indicating a strong k_z dependence due to its bulk nature as predicted in panel (c), while the non-varying shape of the outer hexagram FS confirms its surface state origin.

FIG. 1: (Color) Crystal and electronic structures of Bi_2Te_3 (a) Tetradymite-type crystal structure of Bi_2Te_3, formed by stacking quintuple-layer groups sandwiched by three sheets of Te and two sheets of Bi. (b) Calculated bulk conduction band(BCB) and bulk valance band(BVB) dispersions along high symmetry directions of the surface BZ (see inset), with the chemical potential rigidly shifted to 45meV above the BCB bottom at to match the experimental result. (c) The k_z dependence of the calculated bulk FS projection on the sur-

. Crossover of Three-Dimensional Topological Insulator of Bi_2Se_3 to the

6

Two-Dimensional Limit

Yi Zhang[1], Ke He[1*], Cui-Zu Chang[1,2], Can-Li Song[1,2], Li-Li Wang[1], Xi Chen[2], Jin-Feng Jia[2], Zhong Fang[1], Xi Dai[1], Wen-Yu Shan[3], Shun-Qing Shen[3], Qian Niu[4], Xiao-Liang Qi[5], Shou-Cheng Zhang[5], Xu-Cun Ma[1], and Qi-Kun Xue[1,2*]

Nature Phys. **6**, 584 (2010)

o

4

/

QL	E_0 (eV)	D (eV·Å^2)	Δ (eV)
2	-0.470	-14.4	0.252
3	-0.407	-9.7	0.138
4	-0.363	-8.0	0.070
5	-0.345	-15.3	0.041
6	-0.324	-13.0	0

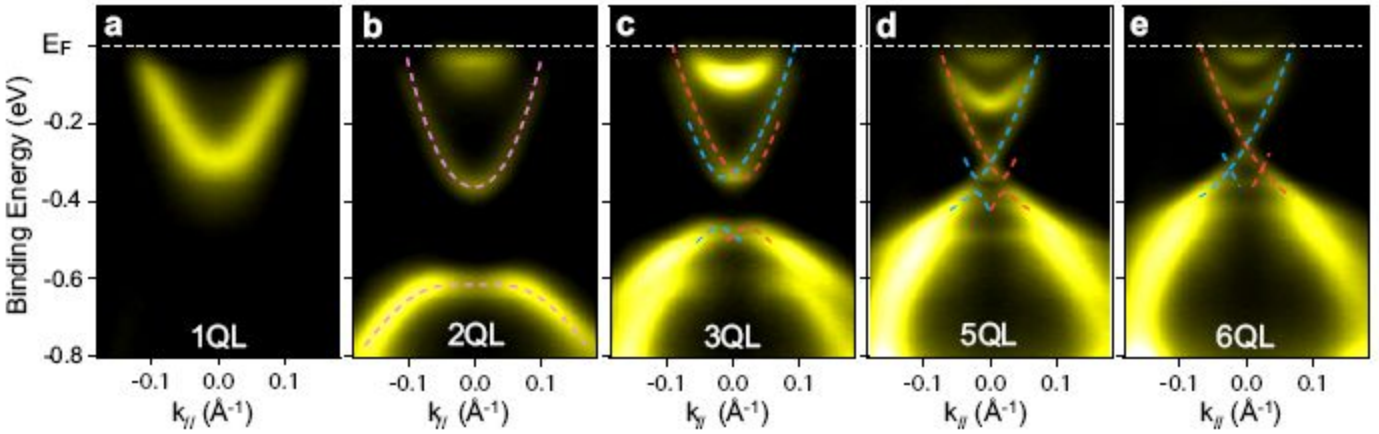

$$E_{\pm}(k_{//}) = E_0 - Dk_{//}^2 \pm \sqrt{(v_F \hbar k_{//})^2 + (\frac{\Delta}{2} - Bk_{//}^2)^2}$$

$$E_{\sigma\pm}(k_{//}) = E_0 - Dk_{//}^2 \pm \sqrt{(|\vec{V}'| + \sigma v_F \hbar k_{//})^2 + (\frac{\Delta}{2} - Bk_{//}^2)^2}$$

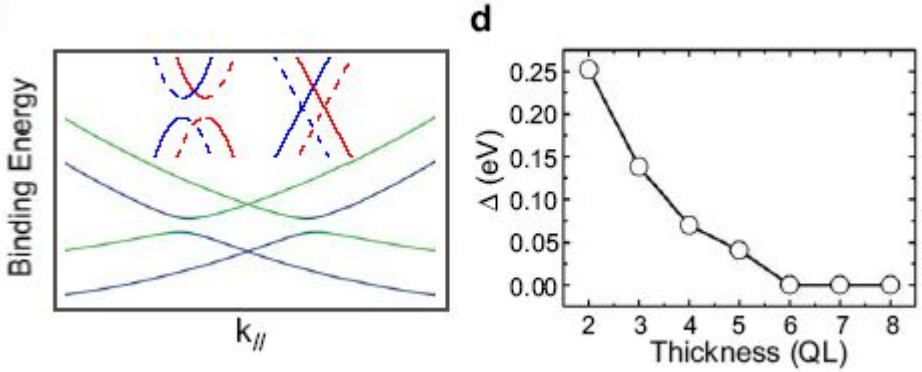

Green and blue colours represent the states that mainly localize at surface and interface, respectively. The inset shows a schematic illustration of the surface states of Bi_2Se_3 film above (right) and below (left) 6 QL. The solid and dashed lines represent the surface states that mainly localize at surface and interface of Bi_2Se_3 film, respectively. The red and blue colours of the lines represent different spins. d

Momentum-Resolved Landau-Level Spectroscopy of Dirac Surface State in Bi_2Se_3

T. Hanaguri,[1] K. Igarashi,[2] M. Kawamura,[1] H. Takagi,[1,3] and T. Sasagawa[2]

Phys Rev B **82**, 081305 (2010)

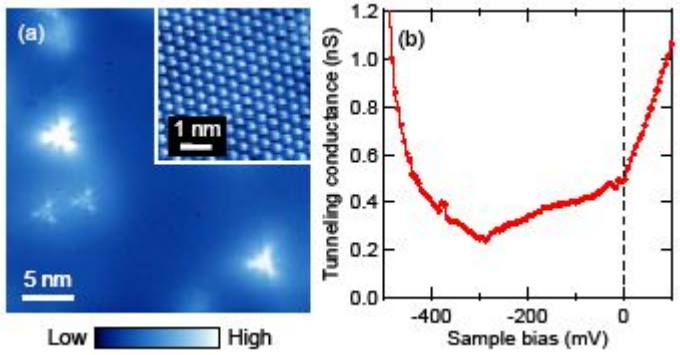

ergy E_n of n-th LL of Dirac fermions is expressed as

$$E_n = E_{DP} + \mathrm{sgn}(n) v \sqrt{2e\hbar|n|B},$$

Here we demonstrate a way to derive the E-k dispersion from the LL spectroscopy. Since the Landau orbit is quantized in k space, we can pick out specific momentum.

According to the Bohr-Sommerfeld quantization condition, the area S_n of the n-th Landau orbit in k space is given by $S_n = (n+\gamma)2\pi eB/\hbar$, where γ is the phase

$$k_n = \sqrt{\frac{2e|n|B}{\hbar}}.$$

Thus, once we specify n and B, a set of E_n and k_n can be obtained. Since $\sqrt{|n|B}$ represents k_n, E_n should be scaled by $\sqrt{|n|B}$ and the scaling function is nothing but the E-k dispersion relation.

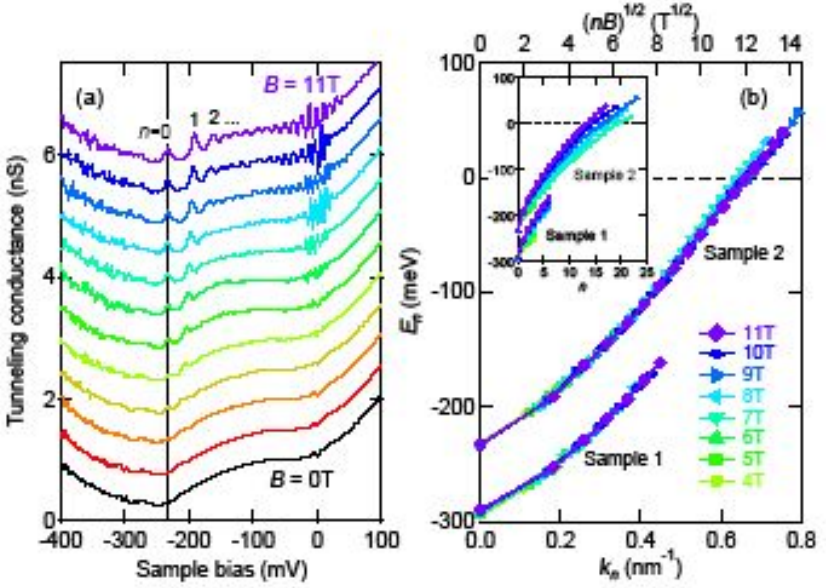

FIG. 3: (color online). (a) Tunneling spectra showing the series of peaks associated with the LL formation. Data were collected in a magnetic field perpendicular to the surface from 0 T up to 11 T with 1 T interval. $V_s = +100$ mV, $I_t = 0.2$ nA

LLs E_n scaled by the square-roots of field B and LL index n. The scaling parameter $\sqrt{|n|B}$ (top axis) can be converted into the momentum k (bottom axis) and the scaling function represents band dispersion. See text for details. The inset shows the n dependence of E_n before the scaling.

Транспортные эксперименты

Nonlocal transport in quantum spin-Hall state in HgTe quantum well

A.Roth,...L. Molenkamp,... S.-C.Zhang Science **325**, 294 (2009),

Aharonov-Bohm interference in topological insulator nanoribbons Hailin PengHailin Peng, Keji LaiHailin Peng, Keji Lai, Desheng KongHailin Peng, Keji Lai, Desheng Kong, Stefan MeisterHailin Peng, Keji Lai, Desheng Kong, Stefan Meister, Yulin Chen, Xiao-Liang Qi Xiao-Liang Qi, Shou-Cheng Zhang Xiao-Liang Qi, Shou-Cheng Zhang, Zhi-Xun Shen Xiao-Liang Qi, Shou-Cheng Zhang, Zhi-Xun Shen, Yi Cui
arXiv:0908.3314

Giant magnetic fingerprint in non-metallic Bi2Se3

J.Checkelsky et al arXiv:0909.1840

Superconductivity in CuxBi2Se3 and its implications for pairing in the undoped topological insulator Y. S. Hor Y. S. Hor, A. J. Williams Y. S. Hor, A. J. Williams, J. G. Checkelsky, P. RoushanP. Roushan, J. SeoP. Roushan, J. Seo, Q. XuP. Roushan, J. Seo, Q. Xu, H. W. ZandbergenP. Roushan, J. Seo, Q. Xu, H. W. Zandbergen, A. YazdaniP. Roushan, J. Seo, Q. Xu, H. W. Zandbergen, A. Yazdani, N. P. OngP. Roushan, J. Seo, Q. Xu, H. W. Zandbergen, A. Yazdani, N. P. Ong, R. J. Cava

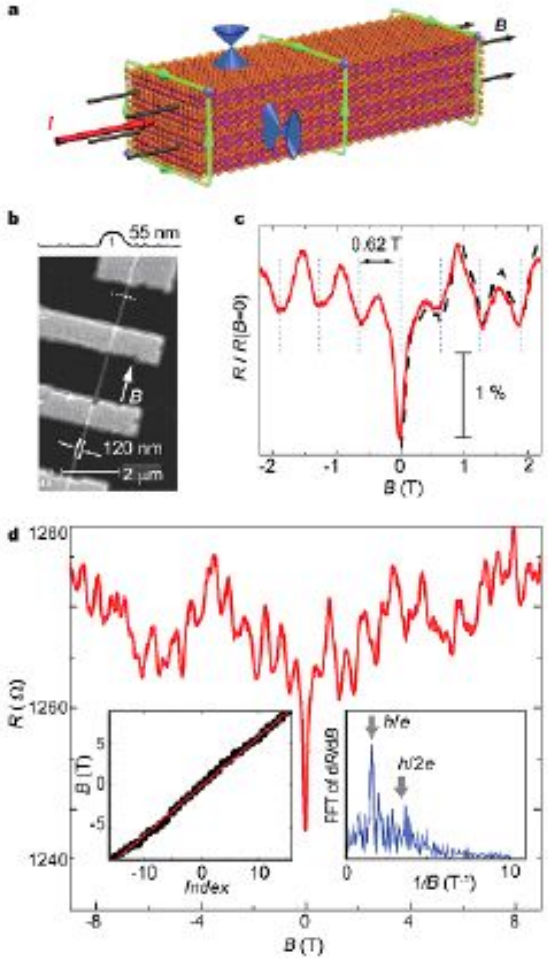

FIG. 2: a. Schematic of a 2D topological surface states of a layered Bi_2Se_3 nanoribbon under a magnetic field along the ribbon length. The red and black arrows correspond to the electric current and magnetic field lines, respectively. The two cones on the top and side surfaces illustrate the Dirac surface states propagating on all surfaces with linear dispersion. The green loops encircling the same magnetic flux stand for phase coherent paths through which the surface electrons interfere. b. SEM image of a Bi_2Se_3 nanoribbon, 120nm in width, contacted by four Ti/Au electrodes. The thickness of the nanoribbon is measured by AFM (a line cut in the inset) to be 55nm. c. Normalized magnetoresistance of the nanoribbon in radial magnetic fields at 2K. A clear modulation of the resistance with a period of 0.62T is observed, corresponding to one flux quantum (h/e) threaded into the cross section of the nanoribbon. The solid red trace (up sweep) was taken with a scan rate of 3mT/sec and the dashed black line (down sweep) at 10mT/sec. d. Magnetoresistance in the full field range of $\pm$9T. Inset on the left, magnetic field position of well developed resistance minima. Inset on the right, Fast Fourier transform (FFT) of the derivative $\mathrm{d}R/\mathrm{d}B$ in the entire field range. Locations of h/e and $h/2e$ flux quantization are labeled.

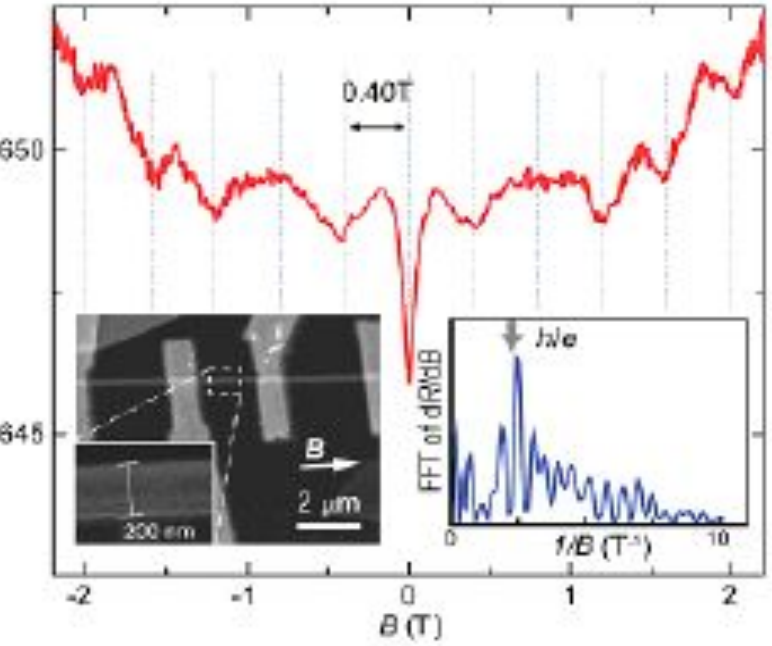

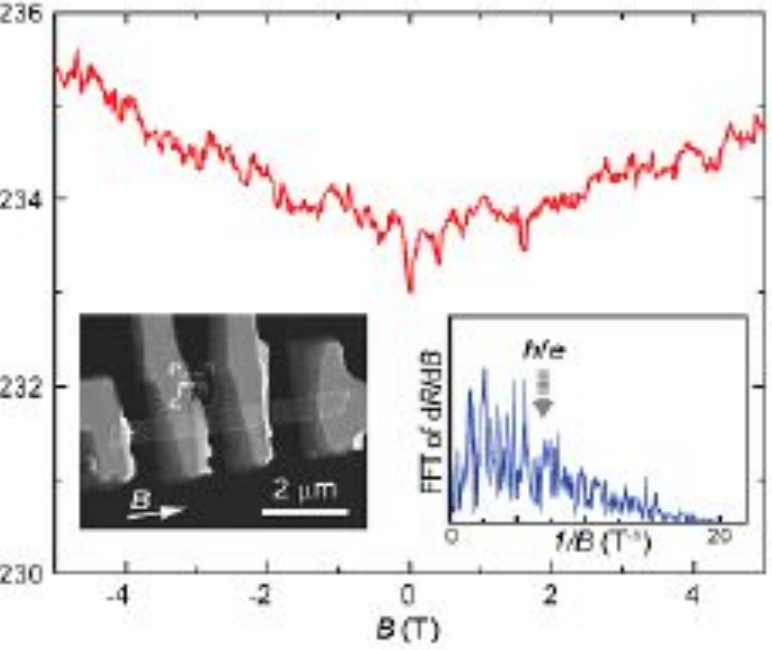

FIG. 4: a. AB oscillations of the nanoribbon shown in the
set. The label of h/e marks the calculated (from the cross s
tion 200nm × 50nm) $1/B$ frequency in the FFT plot. b. A
riodic magnetoresistance of a wide ribbon (570nm × 50n
and the SEM in the inset. The FFT spectrum shows no
parent peaks. The location of h/e is again indicated for co
parison.

Phase and period of oscillations ?

J.Bardarson, P.Brouwer and J. Moore
Phys Rev Lett 105, 156803 (2010)

Giant magnetofingerprint in non-metallic Bi_2Se_3.

J. G. Checkelsky[1], Y. S. Hor[2], M.-H. Liu[1,†], D.-X. Qu[1], R. J. Cava[2] and N. P. Ong[1]

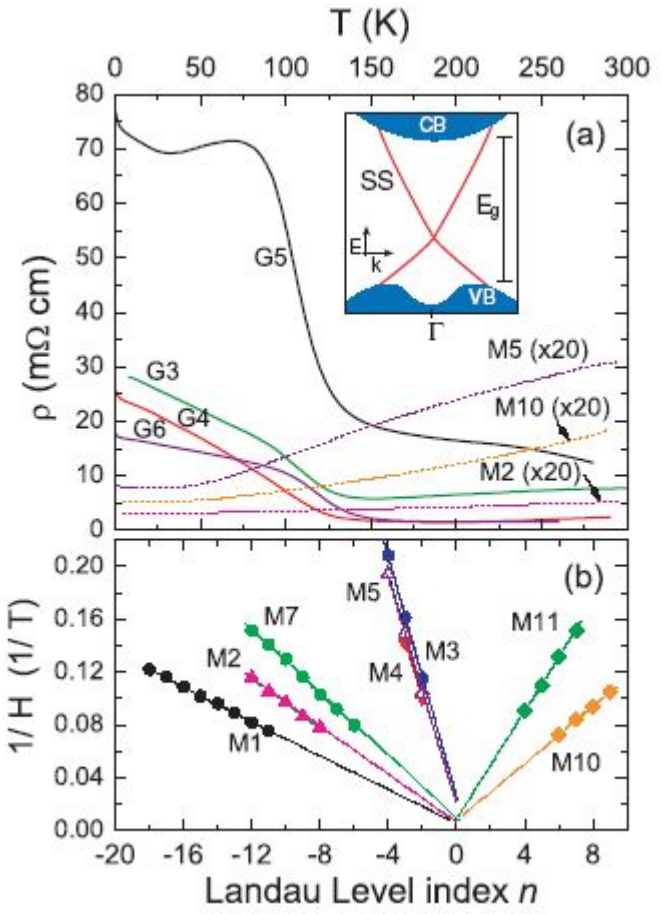

FIG. 1: (a) Resistivity ρ vs. T in 4 samples (G3–G6) of $Ca_xBi_{2-x}Se_3$ lightly doped with Ca to bring μ_b into the gap. Samples with μ_b not inside the gap (M2, M5 and M10) display a metallic T dependence (shown $\times 20$). The inset is a sketch of the surface states [10] crossing the gap from the VB to the CB. (b) The LL index plot vs. field minima in the SdH oscillations observed in 8 metallic samples (M1$\cdots$M11). Negative (positive) index n represents the electron (hole) FS pocket. As μ_b is lowered from the CB to VB, the FS area $\mathcal{A} \sim 1/\text{slope}$ drops to zero before rising again.

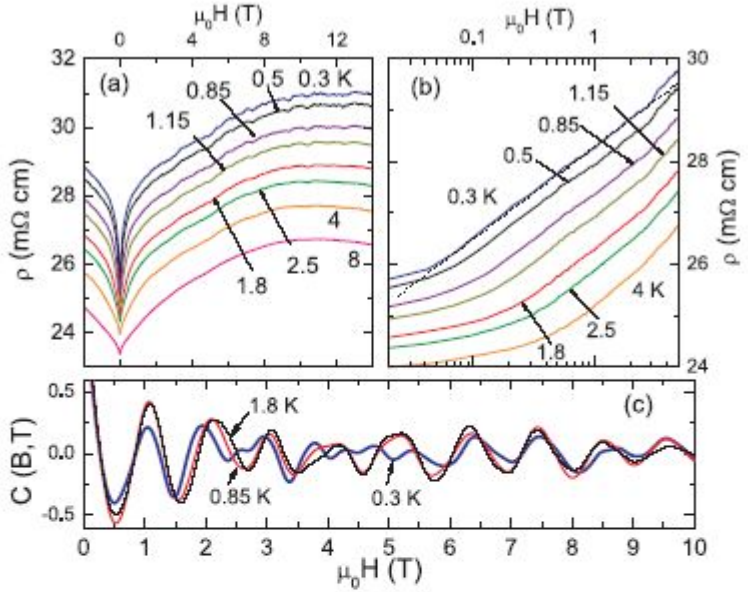

FIG. 2: Curves of ρ vs. H in Sample G4 at 0.3< T <8 K. The curves are plotted vs. H (Panel a) and vs. $\ln H$ (b). The MR displays a sharp anomaly of amplitude 10%R in weak H. In addition, large conductance fluctuations of amplitude up to 0.5% are resolved. In Panel (b), the plot of ρ vs. $\log H$ at 0.3 K shows that $\rho(H) \sim \ln H$ over 2 decades in H (dashed line). The slope is equivalent to $dG/d\ln H = 200e^2/h$. The correlation function $\mathcal{C}(B,T)$ of the fingerprint signals ($\mathbf{H}||\mathbf{z}$) is plotted in Panel (c) for T = 0.3 K (bold curve), 0.85 K (medium) and 1.8 K (thin). $\mathcal{C}(B)$ oscillates vs. H instead of decaying as a power law.

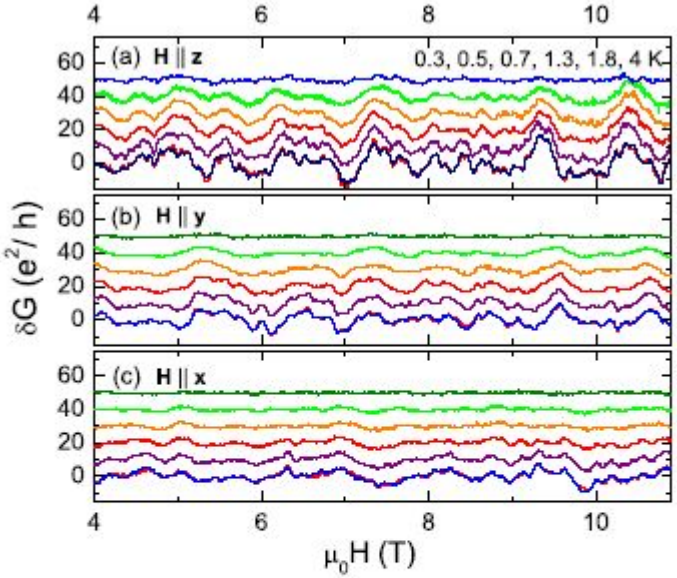

FIG. 3: Curves of the magneto-fingerprint signal $\delta G(T,H)$ vs H in Sample G4. The field $\mathbf{H}$ is aligned with $\hat{\mathbf{z}}$ (in Panel a), with $\hat{\mathbf{y}}$ (in b), and with $\hat{\mathbf{x}}||\mathbf{I}$ (in c). In each panel, curves are shown for five T between 0.3 and 4 K (in ascending order). For clarity, adjacent curves are displaced vertically by 10 e^2/h. At 0.3 K, both up-sweep and down-sweep traces are shown superposed to emphasize retraceability.

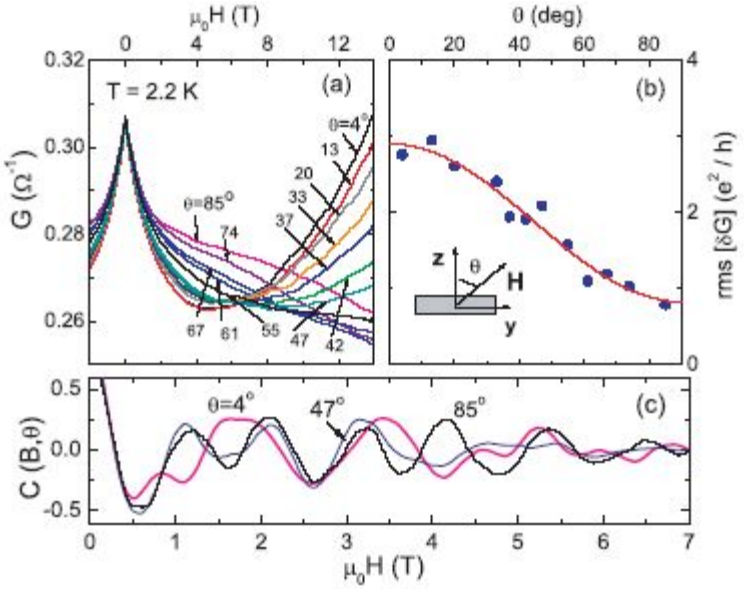

FIG. 4: The magneto-fingerprint signal in tilted field. (Panel a) The MR curves in G4 at selected field-tilt angles $4^\circ < \theta < 85^\circ$ at $T = 2.2$ K. Panel (b) shows the rms amplitude rms$[\delta G]$ vs. tilt angle θ (θ is defined in inset). The fit to rms$[\delta G] = [a + b\cos^2(\theta)](e^2/h)$ yields $a = 0.832$ and $b = 2.08$ (solid curve). Panel (c) plots the correlation function $\mathcal{C}(B)$ vs. H at selected θ.

$$\Delta G(H) = -\frac{e^2}{h}[A_{orb} + A_{spin}] \ \ln H,$$

	ρ	c	G	rmsδG	A	n_H
units	mΩcm	μm	e^2/h	e^2/h		10^{18} cm^{-3}
G3	30	50	-	-	-	0.7
G4	15	50	8,000	5.9	178	5
G5	76	80	1,760	0.8	35	1
G6	18	50	7,000	1	135	7
G7	16	25	4,800	0.9	63	8
G8	25	10	1,050	0.6	20	5

TABLE I: Sample parameters. c is the crystal thickness along c. Values of G and rmsδG (in e^2/h) and ρ are measured at 0.3 K (except for G3, which was not cooled below 4 K). We define $A \equiv A_{orb} + A_{spin}$ (see Eq. 2). The crystals are of nominal size 2 mm$\times$ 2 mm $\times$ c. The Hall density $n_H = 1/eR_H$ is inferred from the Hall coefficient R_H.

Very thin crystals

arXiv:1003.3883

J. G. Checkelsky[1,†], Y. S. Hor[2,‡], R. J. Cava[2] and N. P. Ong[1]

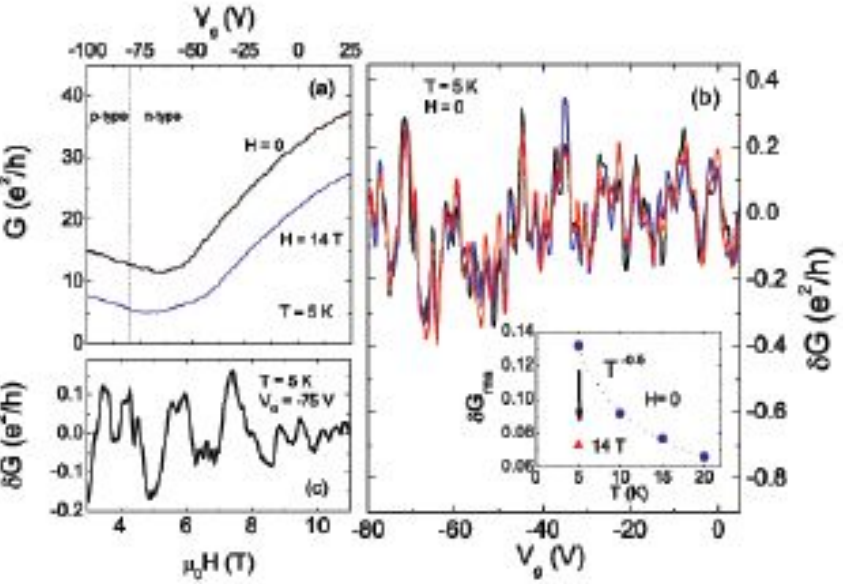

G. 3: (a) Conductance $G(T,0)$ in zero H (upper trace) h $G(T,H)$ at 14 T (lower) at $T = 5$ K for sample S1. the $H = 0$ trace (superposition of 3 traces), retraceable tuations are resolved, though suppressed in the trace at 14 (b) Amplitude of the conductance fluctuation $\delta G = G - \langle G \rangle$ th $\langle G \rangle$ a smooth background) The T dependence of the rms ue δG_{rms} (solid circles in inset) fits well to $T^{-0.5}$ (dashed ve). (c) Fluctuations for V_g =-75 V as a function of H.

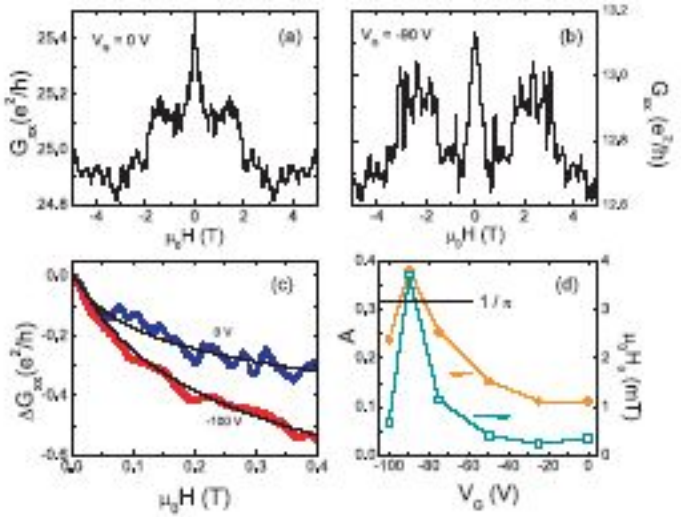

FIG. 4: Panels (a) and (b) show conductance fluctuations for sample S2 in the trace of G vs. H in sample S2 at 0.3 K with V_g fixed at 0 V and at -90 V. (c) Low-H magnetoconductance at $V_g = 0$ V and V_g =-100 V. The solid lines are fits to Eq. 2. (d) A and the dephasing field H_0 show a sharp maximum near the charge-neutral point. Dashed line shows the value $A = 1/\pi$ predicted for dominant spin-orbit coupling (see text).

$$\Delta G_{xx}(H) = A\frac{e^2}{h}\left[\ln\frac{H_0}{H} - \psi\left(\frac{1}{2} + \frac{H_0}{H}\right)\right]$$

Gate-tuned normal and superconducting transport at the surface of a topological insulator

Benjamin Sacépé[1,2§*], Jeroen B. Oostinga[1,2*], Jian Li[3], Alberto Ubaldini[1], Nuno J.G. Couto[1,2], Enrico Giannini[1] & Alberto F. Morpurgo[1,2#]

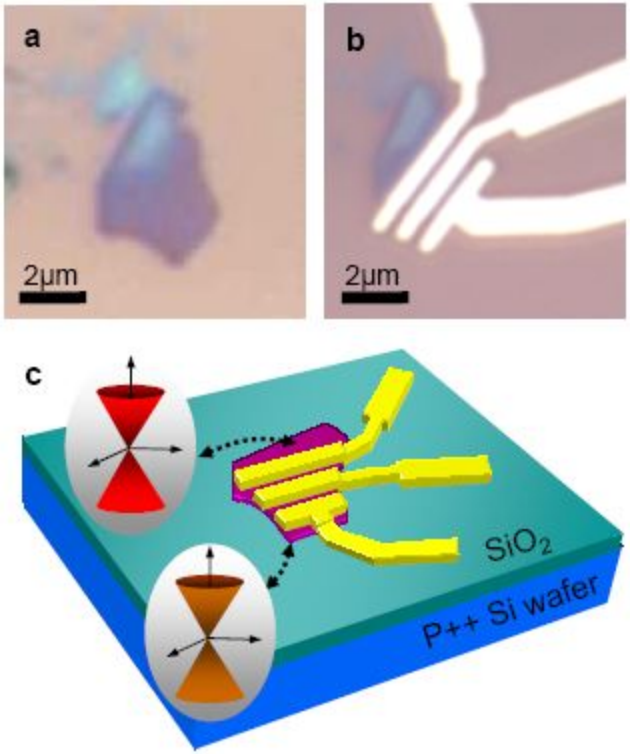

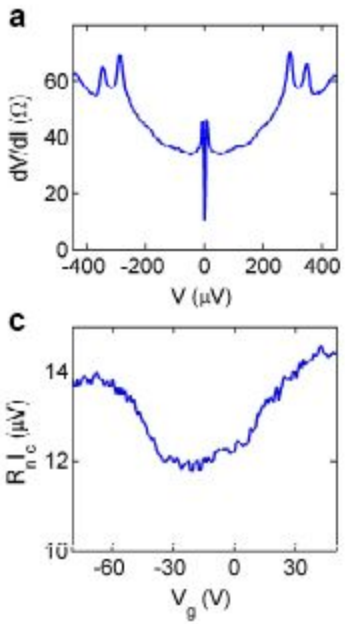

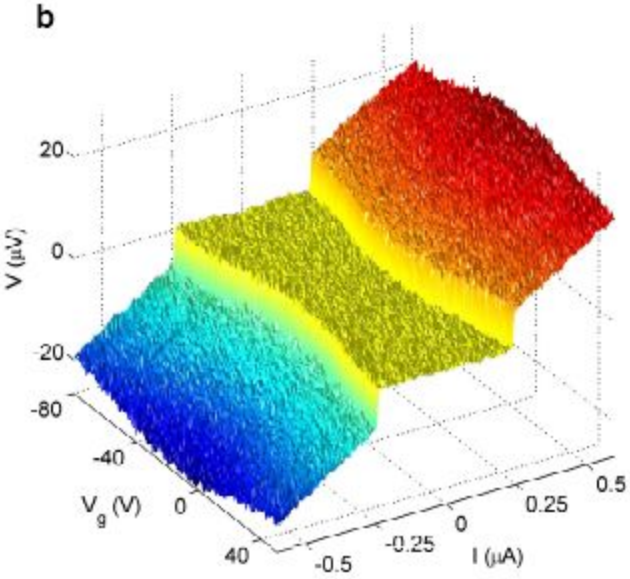

Лекция 2. Теория

- Топологические свойства зонных диэлектриков
- Общая классификация возможных топологических фаз в размерностях d=1,2,3
- Связь с проблемами спиновой жидкости и p_x+ip_y сверхпроводящего состояния
- Майорановские фермионы:

  как напасть на их след

Теория зонных ТИ

J.Moore and L.Balents, PRB **75**, 121306 (2007)
S.Murakami, S.Kuga arxiv:0806.3309
L.Fu and C.Kane PRB **76**, 045302 (2007); ibid **74**, 195312 (2006)

Топологические калибровочные теории

Topological field theory of time-reversal invariant insulators
Xiao-Liang Qi, Taylor L. Hughes and Shou-Cheng Zhang
Phys. Rev. B **78**, 195424 (2008) – Published November 24, 2008

Topological *BF* field theory description of topological insulators

Gil Young Cho[1] and Joel E. Moore[1,2] **Arxiv:1011.3485**

Общая топологическая классификация

A.Kitaev, Periodic table for topological insulators and superconductors, arXiv:0901.2686
A.Ludwig et al, contribution to Landau-100 Conference Proceedings, arxiv: arXiv:0905.2029

Topological Insulators with Inversion Symmetry

Liang Fu and C.L. Kane

Phys Rev B
76, 045302 (2007)
75, 195312 (2006)

Bloch wavefunctions

$$|\psi_{n,\mathbf{k}}\rangle = e^{i\mathbf{k}\cdot\mathbf{r}}|u_{n,\mathbf{k}}\rangle.$$

We require $|\psi_{n,\mathbf{k}+\mathbf{G}}\rangle = |\psi_{n,\mathbf{k}}\rangle$ for reciprocal lattice vectors $\mathbf{G}$, so that the Brillouin zone in which $\mathbf{k}$ is defined is a torus. This implies $|u_{n,\mathbf{k}+\mathbf{G}}\rangle = e^{-i\mathbf{G}\cdot\mathbf{r}}|u_{n,\mathbf{k}}\rangle$. Time reversal symmetry implies $[\mathcal{H}, \Theta] = 0$, where $\Theta = \exp(i\pi S_y)K$

$\Theta^2 = -1$. It follows that $H(-\mathbf{k}) = \Theta H(\mathbf{k})\Theta^{-1}$.

There are special points $\mathbf{k} = \Gamma_i$ in the Brillouin zone which are time reversal invariant and satisfy $-\Gamma_i = \Gamma_i + \mathbf{G}$ for a reciprocal lattice vector $\mathbf{G}$. There are eight such points in three dimensions and four in two dimen-

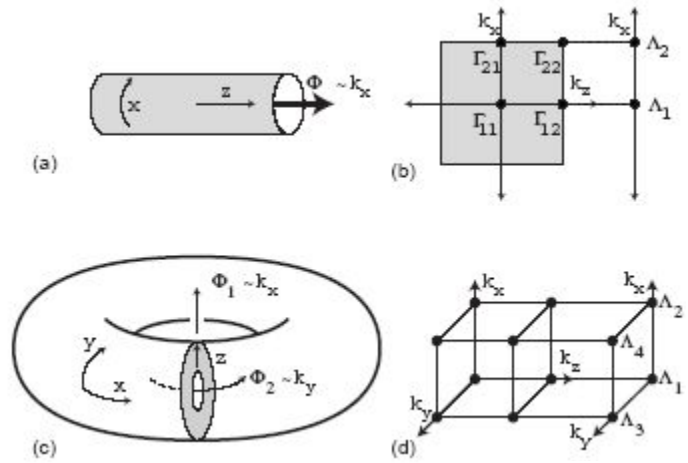

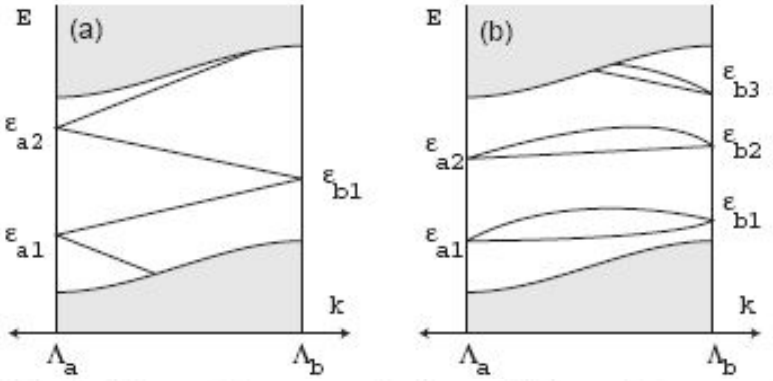

FIG. 2: Schematic representations of the surface energy levels of a crystal in either two or three dimensions as a function of surface crystal momentum on a path connecting Λ_a and Λ_b. The shaded region shows the bulk continuum states, and the lines show discrete surface (or edge) bands localized near one of the surfaces. The Kramers degenerate surface states at Λ_a and Λ_b can be connected to each other in two possible ways, shown in (a) and (b), which reflect the change in time reversal polarization $\pi_a\pi_b$ of the cylinder between those points. Case (a) occurs in topological insulators, and guarantees the surface bands cross any Fermi energy inside the bulk gap.

$$\delta_i = \frac{\sqrt{\det[w(\Gamma_i)]}}{\mathrm{Pf}[w(\Gamma_i)]} = \pm 1,$$

$2N \times 2N$ unitary matrix

$$w_{mn}(\mathbf{k}) \equiv \langle u_{m-\mathbf{k}}|\Theta|u_{n\mathbf{k}}\rangle.$$

$$\langle \Theta a|\Theta b\rangle = \langle b|a\rangle \text{ and } \Theta^2 = -1$$

$$(-1)^{\nu} = \prod_{i=1}^{4} \delta_i.$$

$$(-1)^{\nu_0} = \prod_{i=1}^{8} \delta_i \qquad (-1)^{\nu_k} = \prod_{n_k=1;n_{j\neq k}=0,1} \delta_{i=(n_1 n_2 n_3)}.$$

Topological field theory of time-reversal invariant insulators
Xiao-Liang Qi, Taylor L. Hughes and Shou-Cheng Zhang
Phys. Rev. B **78**, 195424 (2008) – Published November 24, 2008

TRB TOPOLOGICAL INSULATORS IN 2 + 1 DIMENSIONS AND ITS DIMENSIONAL REDUCTION

$$H = \sum_{\mathbf{k}} c^{\dagger}_{\mathbf{k}\alpha} h^{\alpha\beta}(\mathbf{k}) c_{\mathbf{k}\beta} \qquad H \simeq \sum_{\mathbf{k}} c^{\dagger}_{\mathbf{k}} h(\mathbf{k}) c_{\mathbf{k}} + \sum_{\mathbf{k},\mathbf{q}} A^{i}(-\mathbf{q}) c^{\dagger}_{\mathbf{k}+\mathbf{q}/2} \frac{\partial h(\mathbf{k})}{\partial k_i} c_{\mathbf{k}-\mathbf{q}/2}$$

$$\sigma_{xy} = \frac{e^2}{h}\frac{1}{2\pi}\int dk_x \int dk_y f_{xy}(\mathbf{k}) \qquad C_1 = \frac{1}{2\pi}\int dk_x \int dk_y f_{xy}(\mathbf{k}) \in \mathbb{Z}$$

$$\text{with } f_{xy}(\mathbf{k}) = \frac{\partial a_y(\mathbf{k})}{\partial k_x} - \frac{\partial a_x(\mathbf{k})}{\partial k_y}$$

$$a_i(\mathbf{k}) = -i \sum_{\alpha \in \text{ occ}} \langle \alpha \mathbf{k} | \frac{\partial}{\partial k_i} | \alpha \mathbf{k} \rangle, \ i = x, y. \qquad j_i = \sigma_H \epsilon^{ij} E_j$$

$$\rho(B) - \rho_0 = \sigma_H B$$

$$j^{\mu} = \frac{C_1}{2\pi}\epsilon^{\mu\nu\tau}\partial_{\nu}A_{\tau} \qquad S_{\text{eff}} = \frac{C_1}{4\pi}\int d^2x \int dt A_{\mu}\epsilon^{\mu\nu\tau}\partial_{\nu}A_{\tau},$$

$$e = \hbar = 1$$

Example: two band models

$$h(\mathbf{k}) = \sum_{a=1}^{3} d_a(\mathbf{k})\sigma^a + \epsilon(\mathbf{k})\mathbb{I}$$

The occupied band satisfies

$(\mathbf{d}(\mathbf{k})\cdot\sigma)\,|-,\mathbf{k}\rangle = -\,|\mathbf{d}(\mathbf{k})|\,|-,\mathbf{k}\rangle$, which thus corresponds to the spinor with spin polarization in the $-\mathbf{d}(\mathbf{k})$ direc-

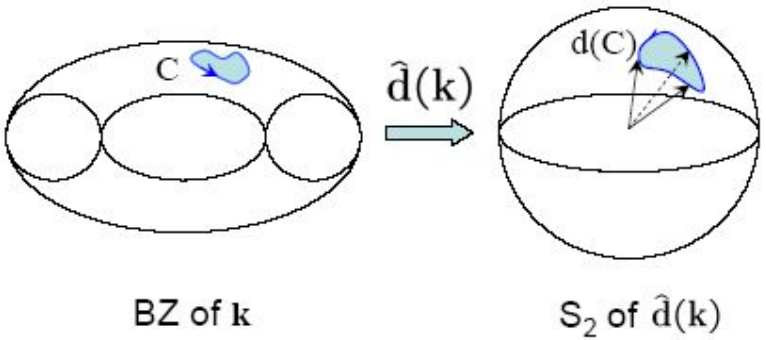

$$C_1 = \frac{1}{4\pi}\int dk_x \int dk_y \hat{\mathbf{d}}\cdot\frac{\partial\hat{\mathbf{d}}}{\partial k_x}\times\frac{\partial\hat{\mathbf{d}}}{\partial k_y}.$$

$$\begin{aligned} h(\mathbf{k}) &= (\sin k_x)\sigma_x + (\sin k_y)\sigma_y \\ &\quad + (m + \cos k_x + \cos k_y)\,\sigma_z, \end{aligned}$$

FIG. 1: Illustration of the Berry's phase curvature in a two-band model. The Berry's phase $\oint_C \mathbf{A}\cdot\mathbf{dr}$ around a path C in the BZ is half of the solid angle subtended by the image path $d(C)$ on the sphere S_2.

$$C_1 = \begin{cases} 1, & 0 < m < 2 \\ -1, & -2 < m < 0 \\ 0, & \text{otherwise.} \end{cases}$$

Непрерывный предел: 0< m +2 << 1

$$h(\mathbf{k}) = \begin{pmatrix} m+2 & k_x - ik_y \\ k_x + ik_y & -m-2 \end{pmatrix}$$

Dimensional reduction

$$H = \sum_n \left[c_n^\dagger \frac{\sigma_z - i\sigma_x}{2} c_{n+\hat{x}} + c_n^\dagger \frac{\sigma_z - i\sigma_y}{2} c_{n+\hat{y}} + h.c. \right] + m \sum_n c_n^\dagger \sigma_z c_n \quad (14)$$

приводит к сумме 1D членов

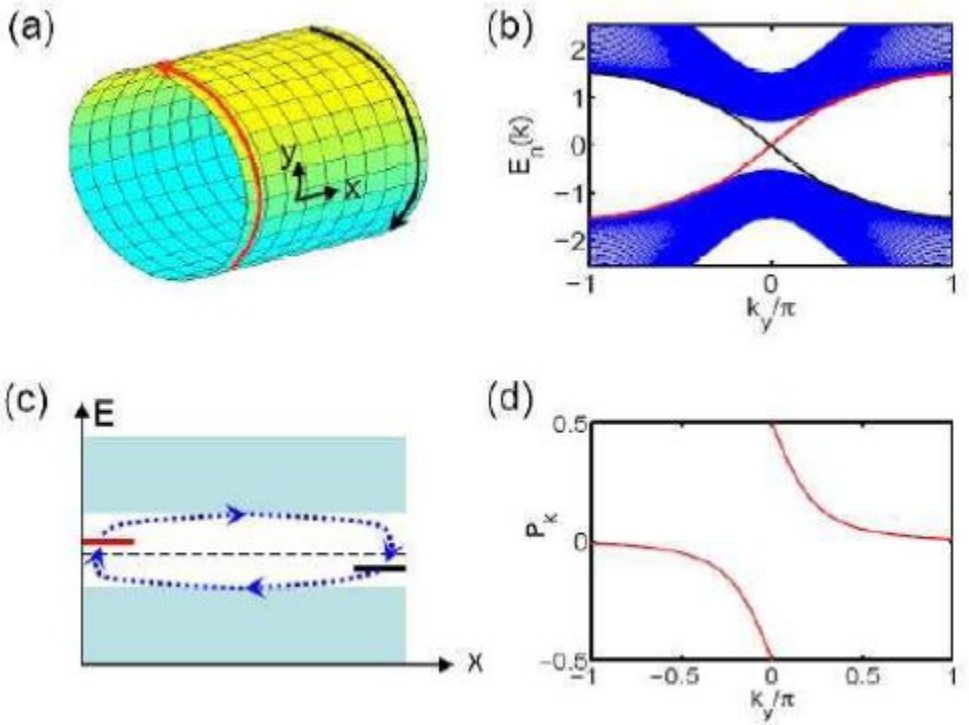

$$H = \sum_{k_y,x} \left[c_{k_y}^\dagger(x) \frac{\sigma_z - i\sigma_x}{2} c_{k_y}(x+1) + h.c. \right] + \sum_{k_y,x} c_{k_y}^\dagger(x) \left[\sin k_y \sigma_y + (m + \cos k_y) \sigma_z \right] c_{k_y}(x)$$

$$A_y = -E_y t, \; A_x = 0.$$

$$\Delta Q = \int_0^{\Delta t} dt \sum_{k_y} J_x(k_y) \equiv \sum_{k_y} \Delta P_x(k_y)|_0^{\Delta t}$$

with $\Delta t = 2\pi/L_y E_y$. In the second equality we use the relation between the current and charge polarization $P_x(k_y)$ of the 1D systems $J_x(k_y) = dP_x(k_y)/dt$. In the

$$\Delta Q = -\oint_0^{2\pi} dk_y \frac{\partial P_x(k_y)}{\partial k_y}. = \sigma_H \Delta t E_y L_y = 2\pi\sigma_H$$ = integer

Topological BF field theory description of topological insulators

Gil Young Cho[1] and Joel E. Moore[1,2]

Topological phases of matter are described universally by topological field theories in the same way that symmetry-breaking phases of matter are described by Landau-Ginzburg field theories. We propose that topological insulators in two and three dimensions are described by a version of abelian BF theory. For the two-dimensional topological insulator or quantum spin Hall state, this description is essentially equivalent to a pair of Chern-Simons theories, consistent with the realization of this phase as paired integer quantum Hall effect states. The BF description can be motivated from the local excitations produced when a π flux is threaded through this state. For the three-dimensional topological insulator, the BF description is less obvious but quite versatile: it contains a gapless surface Dirac fermion when time-reversal-symmetry is preserved and yields "axion electrodynamics", i.e., an electromagnetic $E \cdot B$ term, when time-reversal symmetry is broken and the surfaces are gapped. Just as changing the coefficients and charges of 2D Chern-Simons theory allows one to obtain fractional quantum Hall states starting from integer states, BF theory could also describe (at a macroscopic level) fractional 3D topological insulators with fractional statistics of point-like and line-like objects.

$$S_{3D} = \pm \int d^3x dt \frac{1}{8\pi} \varepsilon^{\mu\nu\lambda\rho} \partial_\mu A_\nu \partial_\lambda A_\rho$$

Магнитоэлектрический эффект
в присутствии щели на пов-сти

Для бесщелевой поверхности выведено
эффективное действие с дираковскими фермионами

i

t

o

n

s

p

Surface States of Topological Insulators: The Dirac Fermion in Curved Two-Dimensional Spaces

Dung-Hai Lee[1,2]

PRL **103,** 196804 (2009)

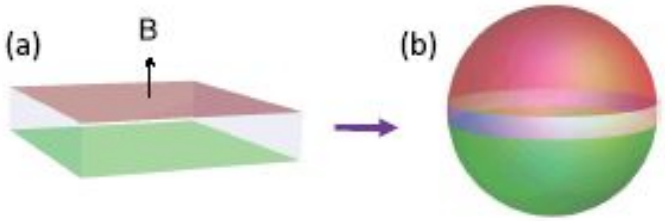

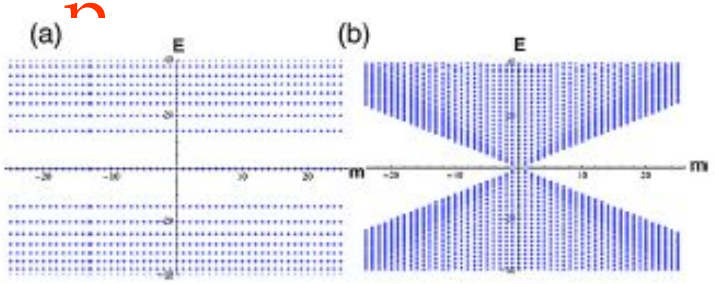

FIG. 2 (color online). The eigenspectra of Eq. (7) under (a) constant magnetic field and (b) zero magnetic field.

that the metric is conformally related to the Euclidean metric everywhere, i.e.,

$$ds^2 = e^{-2\beta(\mathbf{x})}[(dx^1)^2 + (dx^2)^2]. \quad (1)$$

Such a coordinate system is called "isothermal." In terms of isothermal coordinates the Dirac Hamiltonian read

$$H = e^{\beta(\mathbf{x})} \sum_{k=1,2} \sigma_k(\mathbf{x})[-i\partial_k + i\Gamma_k(\mathbf{x}) - iA_k(\mathbf{x})]. \quad (2)$$

In the absence of magnetic field ($n_\phi = 0$) the eigenspectrum is shown as Fig. 2(b). At $m = 0$ there is *one* pair of eigenvalues with $E = 0$, thus there is only one Dirac point. For $n_\phi \gg 1$ the eigenspectrum of Eq. (7) consists of energy levels which are independent of m: $E_n = \pm\sqrt{n(n_\phi + n)/R^2}$ where $n \geq 0$ as shown in the inset of Fig. 2(a). This is the relativistic Landau level on a sphere

Singe Dirac point on the sphere

Как это совместить с открытием щели в тонкой пластинке ?

Туннель для связи с антиподами

Yi ZhangYi Zhang, Ying RanYi Zhang, Ying Ran,
Ashvin Vishwanath arxiv:0904.0690

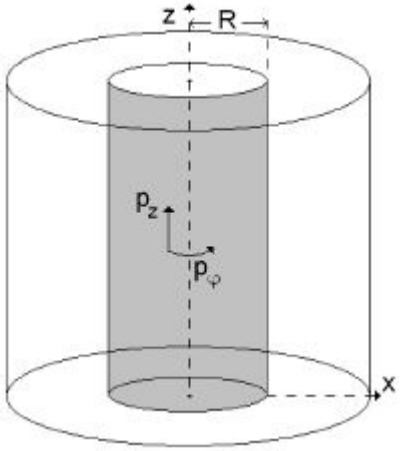

Тонкая бесконечная пластинка ТИ

На верхней и нижней поверхностях живут дираковские электроны

(как в графене, но нет 4-вырождения)

Сквозной туннель радиуса R содержит на внутренней поверхности состояния со спектром

$$E_n^2(k) = \hbar^2(k^2 + n^2/R^2)$$

$n = m + ½ - (\Phi/\Phi_0)$

m – целое число

General classification: A.Kitaev, A.Ludwig et al

Abstract. Gapped phases of noninteracting fermions, with and without charge conservation and time-reversal symmetry, are classified using Bott periodicity. The symmetry and spatial dimension determines a general universality class, which corresponds to one of the 2 types of complex and 8 types of real Clifford algebras. The phases within a given class are further characterized by a topological invariant, an element of some Abelian group that can be 0, $\mathbb{Z}$, or $\mathbb{Z}_2$. The interface between two infinite phases with different topological numbers must carry some gapless mode. Topological properties of finite systems are described in terms of K-homology. This classification is robust with respect to disorder, provided electron states near the Fermi energy are absent or localized. In some cases (e.g., integer quantum Hall systems) the K-theoretic classification is stable to interactions, but a counterexample is also given.

TABLE 1. Classification of free-fermion phases with all possible combinations of the particle number conservation (Q) and time-reversal symmetry (T). The $\pi_0(C_q)$ and $\pi_0(R_q)$ columns indicate the range of topological invariant. Examples of *topologically nontrivial* phases are shown in parentheses.

q	$\pi_0(C_q)$	$d=1$	$d=2$	$d=3$
0	$\mathbb{Z}$		(IQHE)	
1	0			

Above: insulators without time-reversal symmetry (i.e., systems with Q symmetry only) are classified using complex K-theory.

Right: superconductors/superfluids (systems with no symmetry or T-symmetry only) and time-reversal invariant insulators (systems with both T and Q) are classified using real K-theory.

q	$\pi_0(R_q)$	$d=1$	$d=2$	$d=3$
0	$\mathbb{Z}$		no symmetry (p_x+ip_y, e.g., SrRu)	T only (^{3}He-B)
1	$\mathbb{Z}_2$	no symmetry (Majorana chain)	T only $((p_x+ip_y)\uparrow+(p_x-ip_y)\downarrow)$	T and Q (BiSb)
2	$\mathbb{Z}_2$	T only ($(TMTSF)_2X$)	T and Q (HgTe)	
3	0	T and Q		
4	$\mathbb{Z}$			
5	0			
6	0			
7	0			no symmetry

Connections to spin-liquids and p+ip superconductors

Основы:

A.Yu.Kitaev, Ann.Phys. **321**, 2 (2006).
G.Moore and N.Read, Nucl.Phys. **B 360**, 362 (1991).
N.Read and D.Green, Phys. Rev. B **61**, 10267 (2000).
D.Ivanov, Phys.Rev.Lett. **86**, 268 (2001).

Недавние работы

Phys. Rev. B 79, 180501(R) (2009)
Exactly solvable pairing model for superconductors with p_x+ip_y-wave symmetry
M. Ibañez M. Ibañez, Jon Links M. Ibañez, Jon Links, G. Sierra M. Ibañez, Jon Links, G. Sierra, and S.-Y. Zhao

Gauge symmetry in Kitaev-type spin models and index theorems on odd manifolds Yue Yu arXiv:0704.3829 Nucl. Phys. B 799, 345 (2008)

Anyons in an exactly solved model and beyond

Alexei Kitaev

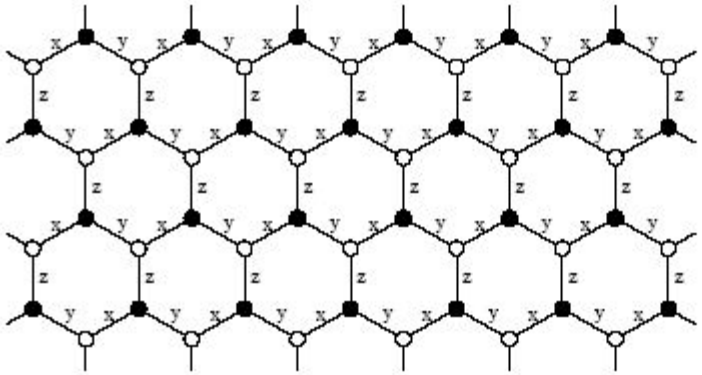

a)

b)

$$H = -J_x \sum_{x\text{-links}} \sigma_j^x \sigma_k^x - J_y \sum_{y\text{-links}} \sigma_j^y \sigma_k^y - J_z \sum_{z\text{-links}} \sigma_j^z \sigma_k^z,$$

All products $W_p = \sigma_1^x \sigma_2^y \sigma_3^z \sigma_4^x \sigma_5^y \sigma_6^z$ commute with H

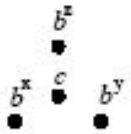

$$\widetilde{\sigma}^x = ib^x c, \quad \widetilde{\sigma}^y = ib^y c, \quad \widetilde{\sigma}^z = ib^z c.$$

Majorana representation

$$H_{\text{vortex-free}} = \frac{i}{4}\sum_{j,k} A_{jk} c_j c_k, \qquad A_{jk} = 2J_{\alpha_{jk}} u_{jk}^{\text{std}}.$$

$$i\widetilde{A}(\mathbf{q}) = \begin{pmatrix} 0 & if(\mathbf{q}) \\ -if(\mathbf{q})^* & 0 \end{pmatrix}, \qquad \varepsilon(\mathbf{q}) = \pm|f(\mathbf{q})|,$$

$$f(\mathbf{q}) = 2\left(J_x e^{i(\mathbf{q},\mathbf{n}_1)} + J_y e^{i(\mathbf{q},\mathbf{n}_2)} + J_z\right),$$

$$\mathbf{q}_* \equiv \tfrac{1}{3}\mathbf{q}_1 + \tfrac{2}{3}\mathbf{q}_2 \pmod{\mathbf{q}_1, \mathbf{q}_2}$$

$$-\mathbf{q}_* \equiv \tfrac{2}{3}\mathbf{q}_1 + \tfrac{1}{3}\mathbf{q}_2 \pmod{\mathbf{q}_1, \mathbf{q}_2}$$

$$(J_x = J_y = J_z)$$

single Dirac fermion mode!

$$\varepsilon(\mathbf{q}) \approx \pm\sqrt{g_{\alpha\beta}\,\delta q_\alpha\,\delta q_\beta},$$

where $\delta\mathbf{q} = \mathbf{q} - \mathbf{q}_*$ or $\delta\mathbf{q} = \mathbf{q} + \mathbf{q}_*$.

gDirac

B-phase can be made gapful

1) Including of magnetic field, or NNN fermionic couplings (Kitaev 2006)

$$i\widetilde{A}(\mathbf{q}) = \begin{pmatrix} \Delta(\mathbf{q}) & if(\mathbf{q}) \\ -if(\mathbf{q})^* & -\Delta(\mathbf{q}) \end{pmatrix}, \qquad \varepsilon(\mathbf{q}) = \pm\sqrt{|f(\mathbf{q})|^2 + \Delta(\mathbf{q})^2},$$

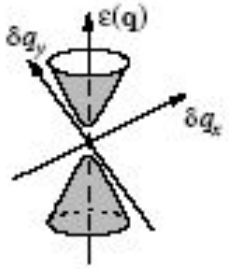

$$\varepsilon(\mathbf{q}) \approx \pm\sqrt{3J^2\,|\delta\mathbf{q}|^2 + \Delta^2},$$

where $\delta\mathbf{q} = \mathbf{q} - \mathbf{q}_*$ or $\delta\mathbf{q} = \mathbf{q} + \mathbf{q}_*$.

Chern number $$\nu = \frac{1}{4\pi}\int \left(\frac{\partial \mathbf{m}}{\partial q_x} \times \frac{\partial \mathbf{m}}{\partial q_y}, \mathbf{m}\right) dq_x\, dq_y = \operatorname{sgn}\Delta = \pm 1.$$

2) Going to decorated honeycomb lattice (Yao-Kivelson 2007)

a

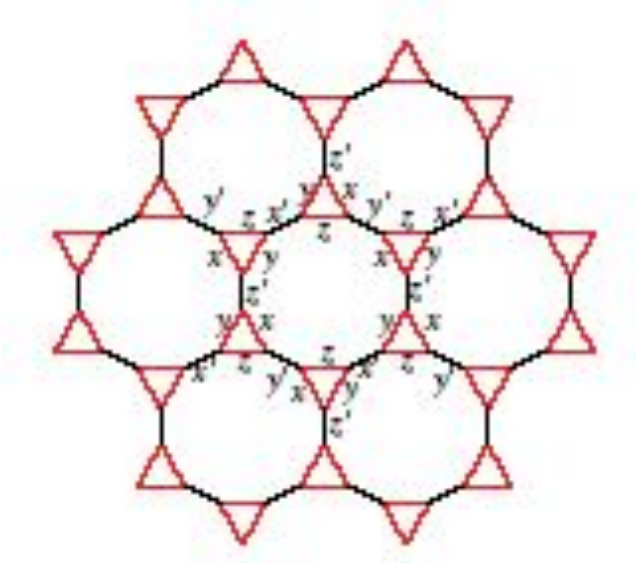

$$\mathcal{H} = \sum_{x\text{-link}} J_x \sigma_i^x \sigma_j^x + \sum_{y\text{-link}} J_y \sigma_i^y \sigma_j^y + \sum_{z\text{-link}} J_z \sigma_i^z \sigma_j^z$$
$$+ \sum_{x'\text{-link}} J'_x \sigma_i^x \sigma_j^x + \sum_{y'\text{-link}} J'_y \sigma_i^y \sigma_j^y + \sum_{z'\text{-link}} J'_z \sigma_i^z \sigma_j^z, \quad (1)$$

Critical point $J' = \sqrt{3}J$

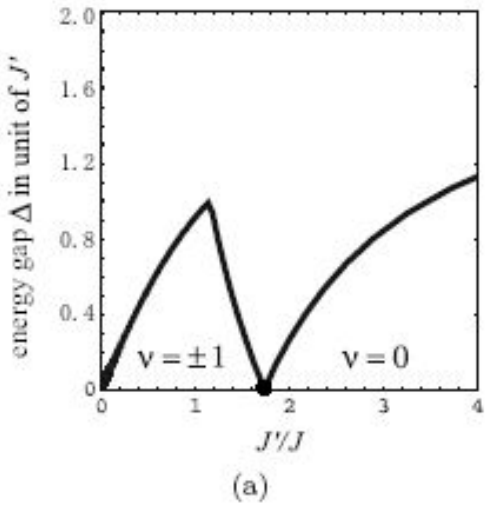

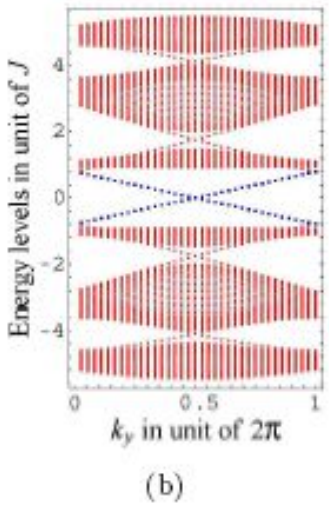

Transition is between topological insulator and trivial insulator

Similar transition was predicted by Read & Green for p-wave superconductors

Майорановские состояния в центрах сверхпроводящих вихрей и неабелева обменная статистика

D.A.Ivanov PRL 2001

$$\Psi(r,\theta) = \Delta(r)\left[e^{i\theta}\,|\uparrow\uparrow\rangle + |\downarrow\downarrow\rangle\right](k_x + ik_y).$$

$$H = \int d^2r \left[\Psi_\uparrow^\dagger \left(\frac{p^2}{2m} - \varepsilon_F\right)\Psi_\uparrow + e^{i\theta}\Delta(r)\Psi_\uparrow^\dagger\left(\nabla_x + i\nabla_y\right)\Psi_\uparrow^\dagger + \text{h.c.}\right].$$

$E_n = n\omega_0$, The zero-energy level becomes a Majorana fermion:

$$\gamma^\dagger(E=0) = \gamma(E=0).$$

$$\tau(T_1) = \exp\left(i\frac{\pi}{4}\sigma_z^{(1)}\right)$$

$$T_i : \begin{cases} c_i & \mapsto & c_{i+1} \\ c_{i+1} & \mapsto & -c_i \\ c_j & \mapsto & c_j \end{cases}$$

$$\tau(T_3) = \exp\left(i\frac{\pi}{4}\sigma_z^{(2)}\right)$$

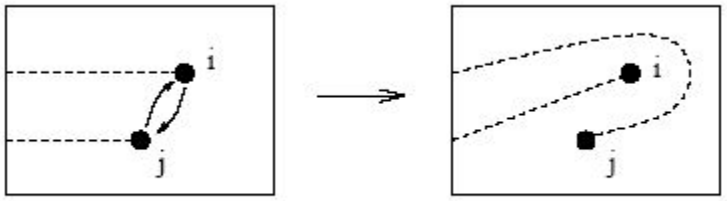

FIG. 3. Elementary braid interchange of two vortices.

4 vortices:
Non-Ab trans.

$$\tau(T_2) = \exp\left(\frac{\pi}{4}c_3c_2\right) =$$

Superconducting Proximity Effect and Majorana Fermions at the Surface of a Topological Insulator

Phys. Rev. Lett. 100, 096407 (2008) L. FuL. Fu and C. L. Kane

$$H_0 = \psi^\dagger(-iv\vec{\sigma}\cdot\nabla - \mu)\psi.$$

Suppose that an s-wave superconductor is deposited on the surface. Due to the proximity effect, Cooper pairs can tunnel into the surface states. This can be described by adding $V = \Delta\psi_\uparrow^\dagger\psi_\downarrow^\dagger + h.c.$ to H_0, where $\Delta = \Delta_0 e^{i\phi}$

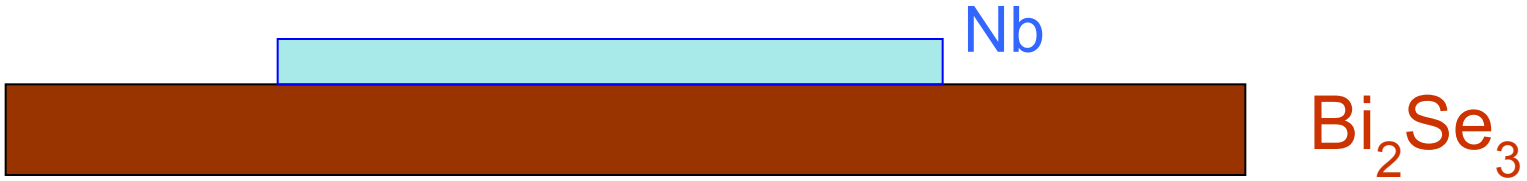

$$H = \Psi^\dagger\mathcal{H}\Psi/2 \qquad \Psi = ((\psi_\uparrow, \psi_\downarrow), (\psi_\downarrow^\dagger, -\psi_\uparrow^\dagger))^T$$

$$\mathcal{H} = -iv\tau^z\sigma\cdot\nabla - \mu\tau^z + \Delta_0(\tau^x\cos\phi + \tau^y\sin\phi).$$

$$E_{\mathbf{k}} = \pm\sqrt{(\pm v|\mathbf{k}| - \mu)^2 + \Delta_0^2}.$$

$$c_{\mathbf{k}} = (\psi_{\uparrow\mathbf{k}} + e^{i\theta_{\mathbf{k}}}\psi_{\downarrow\mathbf{k}})/\sqrt{2}$$

$$\sqrt{2}\tilde{c}_k = \psi_{\uparrow,k}e^{-i\theta_k} - \psi_{\downarrow,k}.$$

Chiral states

Аналогия (неполная) с p_x+ip_y сверхпроводником

$$H = \sum_{\mathbf{k}} (v|\mathbf{k}| - \mu) c^\dagger_{\mathbf{k}} c_{\mathbf{k}} + (\Delta e^{i\theta_{\mathbf{k}}} c^\dagger_{\mathbf{k}} c^\dagger_{-\mathbf{k}} + h.c.)/2 \qquad (1)$$

Time-reversal operator $\Theta = i\sigma^y K \qquad [\Theta, \mathcal{H}] = 0$

$\hat{\Theta}\psi_{\uparrow,k} = -\psi^*_{\downarrow,-k} \quad \hat{\Theta}\psi_{\downarrow,k} = \psi^*_{\uparrow,-k}$ original fermions

$\hat{\Theta}c_k = e^{i\theta_k} c^*_{-k} \quad \hat{\Theta}c^*_k = e^{-i\theta_k} c_{-k}$ chiral fermions

Due to phase factors the current Hamiltonian (1) is T-inv. whereas p_x+ip_y superconductor breaks T-invariance

Сверхпроводящий эффект близости на поверхности ТИ

- С учетом примесного рассеяния на поверхности, которое *не должно* приводить к распариванию (из-за того, что Т-инвариантность не нарушена)

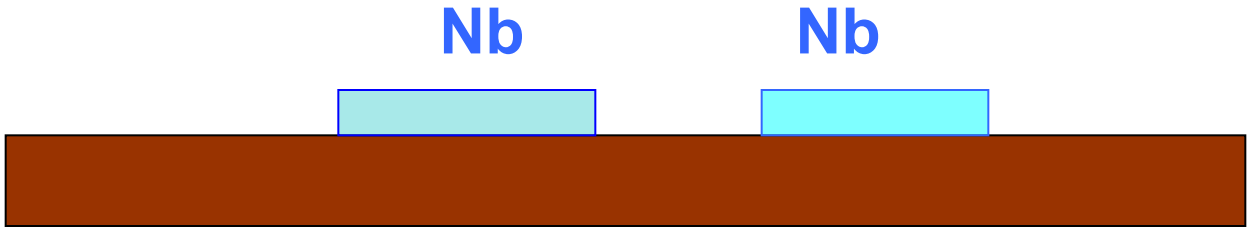

Эксперимент B.Sacepe et al – джозеф. ток на поверхности

Зависимость $I_c(L,T)$ - способ измерить коэфф. диффузии поверхностных состояний

Индуцированная сверхпроводимость и майорановские состояния

- **Superconducting Proximity Effect and Majorana Fermions at the Surface of a Topological Insulator**

  Phys. Rev. Lett. 100, 096407 (2008) L. FuL. Fu and C. L. Kane

Они же: arXiv:0804.4469, arXiv:0903.2427

- **Phys. Rev. Lett. 102, 216404 (2009) Electrically Detected Interferometry of Majorana Fermions in a Topological Insulator** A. R. AkhmerovA. R. Akhmerov, Johan NilssonA. R. Akhmerov, Johan Nilsson, and C. W. J. Beenakker
- **Manipulation of Majorana fermion, Andreev reflection and Josephson current on topological insulators** Yukio TanakaYukio Tanaka, Takehito YokoyamaYukio Tanaka, Takehito Yokoyama, Naoto Nagaosa **arXiv:0907.2088**
- **Majorana Fermion Induced Resonant Andreev Reflection** K. T. Law**Majorana Fermion Induced Resonant Andreev Reflection K. T. Law,** Patrick A. Lee**Majorana Fermion Induced Resonant Andreev Reflection K. T. Law, Patrick A. Lee,** T. K. Ng **arXiv:0907.1909**
- **Detecting Majorana bound states induced by a topological insulator**

Fermionic Hopf solitons and Berry's phase in topological surface superconductors

Ying Ran,[1,2,*] Pavan Hosur,[1] and Ashvin Vishwanath[1,2]

arXiv:1003.1964v2

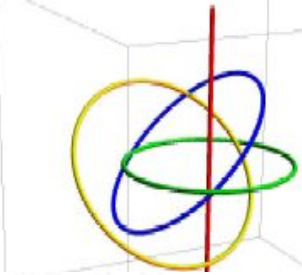

FIG. 1: The Hopf map: $f_H : \vec{r} \to \hat{n}$ is shown by displaying contours of equal $\hat{n}$. Points at infinity are all mapped to the same point on the sphere $f_H(\infty) = \hat{z}$. In red is $f_H^{-1}[\hat{n} = \hat{z}]$, in green $f_H^{-1}[-\hat{z}]$, in blue $f_H^{-1}[\hat{x}]$, and in yellow $f_H^{-1}[\hat{y}]$. Note the unit linking of any pair of curves, which can be used to define the Hopf texture.

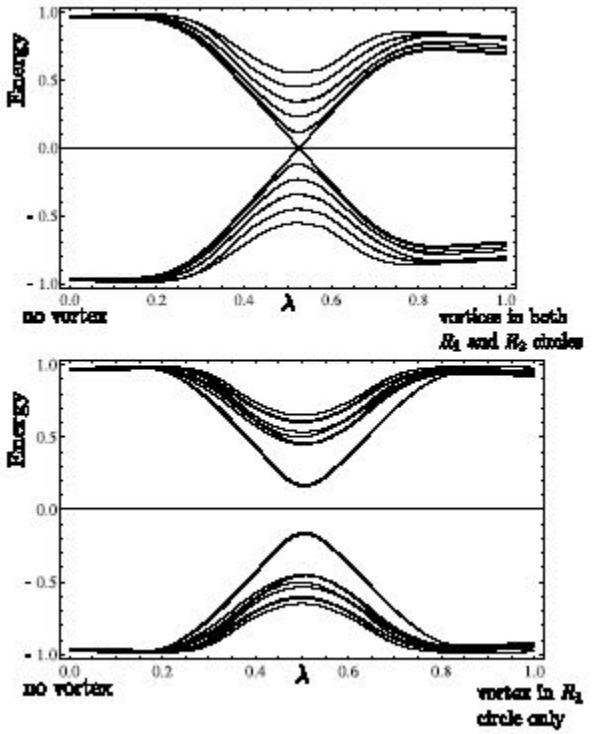

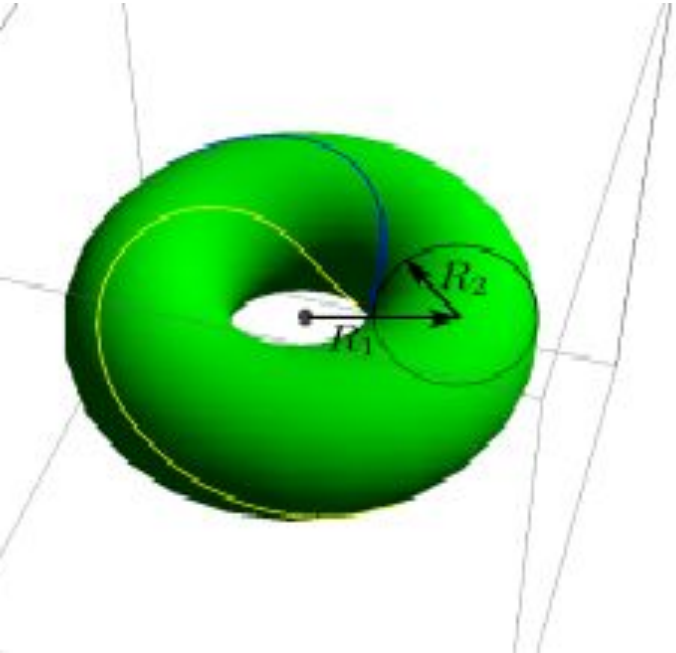

FIG. 3: The spectral flow of the lowest 20 eigenvalues when the pairing on the surface of the topological insulator in Fig. 2 is linearly interpolated between two limits: $\Delta(x, \lambda) = (1 - \lambda)\Delta_0(x) + \lambda\Delta_1(x)$. $\Delta_0(x)$ is constant over the whole surface. TOP: $\Delta_1(x)$ has a unit phase winding (vortex) in both the R_1 and R_2 cycles of the torus, i.e. the Hopf texture. BOTTOM: $\Delta_1(x)$ has a unit phase winding in only the R_1 cycle. It is

Anomalous Josephson current via Majorana bound states in topological insulators

P. A. Ioselevich[1,2] and M. V. Feigel'man[1,2]
[1]*L. D. Landau Institute for Theoretical Physics, Kosygin str.2, Moscow 119334, Russia and*
[2]*Moscow Institute of Physics and Technology, Moscow 141700, Russia*

(PRL, 2011)

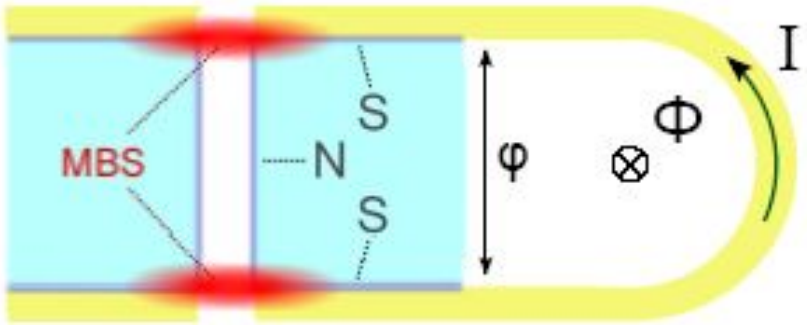

Figure 1: The system: a slab of TI has both surfaces covered by superconductor. A hole channel in the layer hosting a vortex forms an SNS-junction between the surfaces. The superconducting surfaces are connected away from the hole, completing an SNS-circuit with supercurrent flowing through the hole.

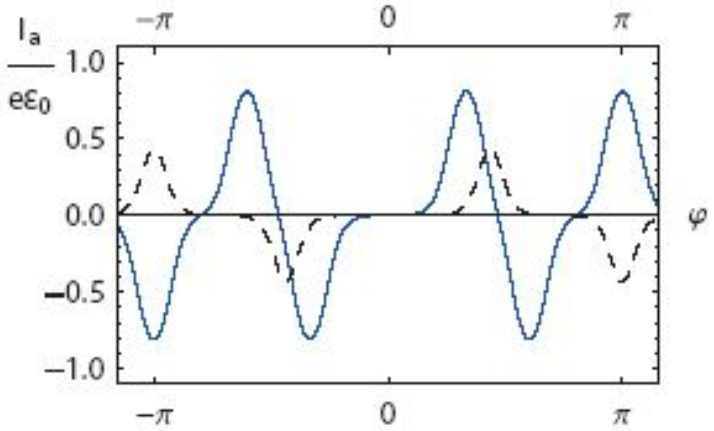

Figure 2: The anomalous current $I_a(\varphi)$ is computed for $p_f R = 2$ (dashed line) and $p_f R = 3$ (blue line). Other parameters are fixed as $p_f \xi = 10$, $p_f \xi_{so} = 5$, $p_f L = 6$, $T = 0.05\Delta$. The extrema of $I_a(\varphi)$ occur whenever a pair of conjugated levels crosses at $\epsilon = 0$.

Parity of the Ground State changes odd number of times while phase φ rotates by 2π whereas fermion parity conserves

The result: 4π – periodic Josephson current